Soliton-antisoliton configurations and the linear and nonlinear optical response of degenerate-ground-state conjugated polymers

T. W. Hagler and A. J. Heeger

Department of Physics and Institute for Polymers and Organic Solids, University of California, Santa Barbara, Santa Barbara, California 93106

(Received 4 November 1992; revised manuscript received 30 August 1993)

The contributions of soliton-antisoliton ($S\bar{S}$) configurations to the linear and third-order nonlinear optical response are investigated for conjugated polymers having a degenerate ground state. We treat the direct photoproduction of charged solitons as a nonlinear Franck-Condon problem and obtain analytical expressions for the linear optical susceptibility $\chi^{(1)}(\omega)$. With the help of the oscillator strength sum rule, we decompose the $\pi-\pi^*$ oscillator strength into two parts; a contribution where the final states are charged $S\bar{S}$ pairs and a contribution where the final states are free electron-hole pairs (as in the noninteracting rigid lattice). The linear optical coefficients calculated from $\chi^{(1)}(\omega)$ are in general agreement with optical data obtained from *trans*-polyacetylene. The results imply that approximately 25% of the integrated oscillator strength of *trans*-polyacetylene arises from the direct photoproduction of solitons. A parallel treatment of the generalized third-order nonlinear optical susceptibility $\chi^{(3)}(\omega_\sigma)$ is presented, demonstrating that, for any third-order process, contributions arising from neutral $S\bar{S}$ pair configurations as intermediate states are one to two orders of magnitude larger than the corresponding rigid-lattice contribution. This mechanism for $\chi^{(3)}$ is enabled by nonlinear zero-point motion which provides a finite Franck-Condon overlap between the ground and $S\bar{S}$ excited state lattice wave functions. The large contribution to $\chi^{(3)}$ from the $S\bar{S}$ intermediate states results from the large transition dipole moment between the free electron-hole pair excited states of B_u symmetry and the A_g symmetric neutral $S\bar{S}$ excited state. This enhanced transition dipole moment is a consequence of the large virtual shifts of oscillator strength associated with the localized $S\bar{S}$ electron-lattice configuration. The third-harmonic conversion efficiency $\chi^{(3)}(3\omega)$ is further enhanced by a condition unique to degenerate-ground-state systems, simultaneous two- and three-photon resonance.

I. INTRODUCTION

A. Ground state symmetry and the nonlinear optical response

Frequency dependent third-harmonic generation (THG) measurements on *cis*- and *trans*-polyacetylene have demonstrated that $\chi^{(3)}(3\omega)$ for *trans*-$(CH)_x$ is an order of magnitude larger than that for the *cis*-isomer over the entire spectral range, even comparing the respective three-photon resonances.[1,2] By measuring THG on oriented free standing films of *trans*-$(CH)_x$, Halvorson *et al.*[3] obtained $\chi^{(3)}(3\omega)$ values in excess of 10^{-7} esu, two orders of magnitude greater than nonoriented *cis*-$(CH)_x$, or any other nondegenerate-ground-state polymer.[4–8] The traditional dependence of $\chi^{(3)}$ on the $\pi-\pi^*$ energy gap obtained from noninteracting rigid-lattice models (NRL),[9–14] i.e., $\chi^{(3)} \sim E_g^{-6}$, does not explain the observed order of magnitude enhancement in $\chi^{(3)}(3\omega)$ achieved by thermal isomerization; $(E_g^{cis}/E_g^{trans})^6 \sim 3$. Furthermore, within the rigid-lattice approximation, the effects of electron-electron interactions are expected to be similar in the two polyacetylene isomers since the sp^2p_z hybridization and the π-electron density are essentially identical. The THG data, therefore, demonstrate a symmetry specific mechanism favoring the degenerate-ground-state system, consistent with the existence of an important contribution to the third-order nonlinear optical susceptibility from virtual $S\bar{S}$ electron-lattice configurations ($S\bar{S}$ pairs) enabled by nonlinear zero-point motion.[15]

B. Ground state symmetry and the linear optical response

The effects of ground state lattice symmetry and nonlinear zero-point motion are observed in the linear optical properties as well. Using a variety of experimental techniques, Lauchlan *et al.*[16,17] performed a comparative investigation of *cis*- and *trans*-polyacetylene, and demonstrated the following isomeric characteristics for the *nondegenerate ground state: cis*-$(CH)_x$ (i) a sharp absorption onset and well-defined vibronic structure, (ii) no measurable photoconductivity, and (iii) band-edge photoluminescence with a Stokes shift of 0.15 eV; and for the *degenerate ground state: trans*-$(CH)_x$ (i) a broad absorption spectrum, distinct low-energy shoulder, and "band tailing" extending deep into the gap, (ii) a three-order-of-magnitude increase in the photoconductivity relative to "*cis*"-$(CH)_x$, and (iii) the absence of band-edge photoluminescence.

When making the *cis*/*trans* experimental comparison, one must first use an effective-medium correction to deconvolve the *true cis*-$(CH)_x$ optical data from the *mea-*

sured "*cis*"-$(CH)_x$ spectrum due to the presence of an inevitable volume fraction of the more thermodynamically stable *trans* isomer. The spectral signature of partial *trans* conversion are readily observed in the linear absorption[16,18,19] and reflectivity spectra.[20] In the third-order nonlinear response, partial *trans* conversion results in two distinct spectral regions in the electroabsorption spectra,[21,22] and in an antiresonance in the THG spectrum.[2,3]

Once the effective-medium correction has been made, the absorption spectrum of *cis*-$(CH)_x$ is found to be characterized by a very sharp onset and well-defined vibronic structure, similar to other nondegenerate-ground-state polymers.[23] In contrast, the *trans*-$(CH)_x$ absorption line shape is broad with a pronounced shoulder on the leading edge and band-tailing, which extends deep into the gap. Although one might argue that the subgap absorption in *trans*-$(CH)_x$ is caused by disorder,[24] x-ray diffraction studies yield Bragg peaks which are significantly narrowed in highly oriented samples.[25] Nevertheless, the subgap absorption features are observed most clearly in data obtained from such highly oriented, structurally ordered samples.[20,22,26]

The photoconductivity action spectrum[16,17] indicates that the subgap optical absorption in *trans*-$(CH)_x$ leads to charge separation: a result consistent with both the Su-Schrieffer mechanism[27] and the direct photoproduction of charged solitons.[28–32] The photoconductivity increases exponentially in the subgap range and shows a well-defined shoulder at 1.5 eV, above which the photocurrent increases much more slowly. In contrast, the as-grown "*cis*"-$(CH)_x$ samples showed little evidence of photogenerated free carriers at any pump energy; the photoconductivity in "*cis*"-$(CH)_x$ samples with a volume fraction of less than 20% *trans* was below experimental resolution.[16,17]

The photoluminescence excitation spectrum demonstrates that, for instantaneous optical processes such as absorption and third-harmonic generation, *cis*-$(CH)_x$ is accurately described as a rigid lattice; the 0.15 eV Stokes shift and the relatively sharp excitation threshold demonstrate that the ground state lattice wave function does not overlap the relaxed configuration of the luminescent polaron exciton. If the nonlinear Franck-Condon factor was of any significance, the relaxed configuration of the polaron exciton could be excited directly and a subgap excitonic feature would be visible in the linear absorption spectrum.[33] For *pure cis*-$(CH)_x$, there is no evidence of significant subgap optical absorption and certainly no evidence of a sharp absorption resonance at the photoluminescence energy. We therefore conclude that in *cis*-$(CH)_x$ the nonlinear component of the lattice zero-point motion is quenched by the nondegenerate ground state.

These results are indicative of a symmetry specific mechanism, which for the degenerate ground state favors charge separation and for the nondegenerate ground state favors polaron-exciton confinement and radiative recombination. The data obtained from the *cis*/*trans* comparative study are consistent with the existence of an important contribution to the linear susceptibility in degenerate-ground-state systems from the direct photoproduction of charged $S\bar{S}$ electron-lattice configurations enabled by nonlinear zero-point motion and this charge separation mechanism is quenched in *cis*-$(CH)_x$ due to the nondegenerate ground state.

C. The role of quantum lattice fluctuations in the linear and nonlinear response

In this paper, we examine the role of quantum lattice fluctuations in both the linear and third-order nonlinear optical susceptibility $\chi^{(1)}(\omega)$ and $\chi^{(3)}(\omega_\sigma)$ within the framework of the continuum version of the Su-Schrieffer-Heeger (SSH) model[34] and the Takayama–Lin-Liu–Maki (TLM) model.[35–37] In our approach, the localized electronic wave function of the $S\bar{S}$ intermediate state is defined in terms of the eigenstates of the perfectly dimerized lattice using a two-particle effective-mass approximation[38,39] and the quantum lattice fluctuations in the degenerate ground state are described by a single collective configurational coordinate representing simultaneously the separation, coherence length, and number density of virtual soliton-antisoliton pairs on the polymer chain. Using this model, we obtain analytical expressions for the linear and third-order nonlinear optical susceptibilities for both the perfectly dimerized (classical) infinite chain and the infinite chain with nonlinear zero-point motion. In our analysis of the linear susceptibility, we demonstrate that $\pi - \pi^*$ oscillator strength is conserved for all $S\bar{S}$ electron-lattice configurations and that the direct photoproduction of charged soliton pairs accounts for roughly 25% of the total integrated oscillator strength in conjugated polymers with a degenerate ground state. For the nonlinear susceptibility, we show that terms in the perturbation theory expansion for $\chi^{(3)}(\omega_\sigma)$ involving neutral $S\bar{S}$ configurations with A_g symmetry as intermediate states are one to two orders of magnitude larger than the corresponding rigid-lattice contribution. The large magnitude of the contribution to the nonlinear response from the neutral $S\bar{S}$ pair intermediate state results from the enhanced transition dipole moment, a consequence of the large (virtual) shifts in oscillator strength required to form the localized electronic wave functions associated with the bond-alternation domain walls. The nonlinear susceptibility for third-harmonic generation $\chi^{(3)}(3\omega)$ is further enhanced by simultaneous two- and three-photon resonance: a condition which is unique to conjugated polymers with a degenerate ground state and strategically designed inorganic quantum-well systems.[41]

In Sec. II the results of time-dependent perturbation theory are reproduced for the case of a one-dimensional electronic system of C_{2h} spatial symmetry interacting with a frequency dependent radiation field; these equations form the basis for the comparison between the NRL model and models containing A_g symmetry states other than the ground state and the doubly occupied Bloch orbitals. In Secs. III and IV the $S\bar{S}$ electron-lattice intermediate states are defined and the nonlinear Franck-Condon factor is evaluated in terms of the ground state lattice wave function. In Sec. V a model is developed for the ground-state lattice wave function in which the

anharmonic quantum lattice fluctuations of the ground state are described as an effective density of virtual soliton-antisoliton pairs. In Sec. VI the linear susceptibility $\chi^{(1)}(\omega)$ is calculated for both the perfectly dimerized infinite chain and the infinite chain with nonlinear zero-point motion, demonstrating that the direct photoproduction of charged soliton pairs accounts for approximately 25% of the total integrated oscillator strength in conjugated polymers with a degenerate ground state. Using typical SSH parameters,[42] we calculate the linear optical absorption coefficient, and find it to be consistent with that obtained from optical measurements on oriented *trans*-$(CH)_x$.[20,26] In Sec. VII an expression for the generalized third-order nonlinear susceptibility is derived for both the noninteracting rigid lattice and the degenerate ground-state system supporting $S\bar{S}$ type excitations, and the frequency dependence of that component of the tensor responsible for third-harmonic generation $\chi^{(3)}(3\omega)$ is computed. Throughout the paper, issues of a technical nature as well as units and dimensions are deferred to the Appendixes.

II. TIME-DEPENDENT PERTURBATION THEORY

A. The linear and third-order nonlinear optical susceptibilities

To evaluate the SSH and TLM linear and nonlinear optical susceptibility, we utilize the results of time-dependent perturbation theory as presented by Orr and Ward.[43] For a system with C_{2h} symmetry, the linear susceptibility is given as

$$\chi^{(1)}(\omega) = e^2 \frac{1}{V} \sum_l \langle g|\mathbf{r}|l\rangle\langle l|\mathbf{r}|g\rangle \left[\frac{1}{(\omega_{lg} - \omega)} + \frac{1}{(\omega_{lg}^* + \omega)} \right], \tag{1}$$

where $|g\rangle$ is the A_g symmetric many-body ground state and the sum over $|l\rangle$ involves only those configurations with B_u symmetry.

The dominant terms in the corresponding expansion for the generalized third-order nonlinear optical susceptibility $\chi^{(3)}(\omega_\sigma = \omega_1 + \omega_2 + \omega_3)$ are given by

$$\chi^{(3)}(\omega_\sigma) = e^4 \frac{1}{V} \sum_l \sum_m \sum_n \frac{\langle g|\mathbf{r}|l\rangle\langle l|\mathbf{r}|m\rangle\langle m|\mathbf{r}|n\rangle\langle n|\mathbf{r}|g\rangle}{(\omega_{lg} - \omega_\sigma)(\omega_{mg} - \omega_1 - \omega_2)(\omega_{ng} - \omega_1)} - e^4 \frac{1}{V} \sum_l \sum_n \frac{\langle g|\mathbf{r}|l\rangle\langle l|\mathbf{r}|g\rangle\langle g|\mathbf{r}|n\rangle\langle n|\mathbf{r}|g\rangle}{(\omega_{lg} - \omega_\sigma)(\omega_{lg} - \omega_3)(\omega_{ng} - \omega_1)} \tag{2}$$

where, in the first term, the intermediate states $|m\rangle$ are any A_g states other than the ground state, and in the second term, only the ground state is considered as the intermediate A_g state.

B. Relevant intermediate states

The linear and nonlinear optical susceptibilities presented in Secs. VI and VII are calculated using the following intermediate states (see Appendixes C and D): *intermediate state* $|l\rangle$: (i) a free electron-hole pair with wave vector k, $|K_I\rangle$ and (ii) a B_u symmetric $S\bar{S}$ electron-lattice configuration $|S\bar{S}^{\pm}\rangle$; *intermediate state* $|m\rangle$: (i) the ground state $|G\rangle$, (ii) a doubly occupied conduction band orbital $|K_{II}\rangle$, and (iii) an A_g symmetric $S\bar{S}$ electron-lattice configuration $|S\bar{S}^0\rangle$; and *intermediate state* $|n\rangle$: (i) a free electron-hole pair with wave vector q $|Q_I\rangle$ and (ii) a B_u symmetric $S\bar{S}$ electron-lattice configuration $|S\bar{S}^{\pm}\rangle$.

There are N B_u symmetric vertical free electron-hole pair excited states $|K_I\rangle$ labeled by the N allowed $(\sigma + k)$ states of the infinite polyene chain, where σ and k are the electron spin and momentum degrees of freedom, respectively. There are, furthermore, $N(N - \xi_0/a)/2$ distinct geometrical configurations for the virtual $S\bar{S}$ pair, each with a different center of mass coordinate Y along the chain and for each center of mass coordinate, the solitons comprising the $S\bar{S}$ pair can be separated by a distance R, with $\xi_0 \leq R \leq Na/2$, where $\xi_0 \approx 7a$ is the coherence length of an isolated soliton: approximately seven carbon-carbon spacings along the chain.[42] Note that in our coordinate system the chain direction, and therefore, the dipole moment, is along the $\mathbf{y}$ axis: $\mathbf{r} \Rightarrow \mathbf{y}$.

Recent theoretical work has emphasized the importance of intraband or "exciton-migration" terms to the nonlinear optical properties of *trans*-polyacetylene.[44] In Appendix F we show that, while the interband transition strength is actually enhanced by relaxing momentum conservation, an exact cancellation occurs when summing the intraband terms in the SSH/TLM model as a direct result of charge conjugation symmetry. The lack of a significant intraband contribution to the third-order nonlinear susceptibility has been confirmed experimentally by the absence of a third-derivative component to the electroabsorption line shape.[21,22,45] We also omit any contributions to the third-order hyperpolarizibility which are proportional to N^2, since these terms correspond to disconnected diagrams and, again, cancel exactly.[46]

III. $S\bar{S}$ INTERMEDIATE STATES

In conjugated polymers, the configurational coordinate coupled most strongly to the π-electronic system is the change in the staggered order parameter: $u_{n+1} - u_n = (-1)^n u_0 + \delta u_n$.[42] The configurational coordinate δu_n describes the local deformation in the bond alternation order parameter, $\Delta(y)$; the latter has been modeled in the continuum limit as bound soliton-antisoliton pairs of separation R:[36,37]

$$\Delta_s(y) = \Delta_0(1 + \tanh(K_0 R)\ \{\tanh[K_0(y - y_0 - Y)] - \tanh[K_0(y + y_0 - Y)]\}), \tag{3}$$

where $\xi(R) = K_0^{-1}$ defines the localization length of the individual bond-alternation defects, or kinks, centered at $Y \pm y_0$, $R = 2y_0$ is the physical separation between the two solitons along the chain ($\hat{\mathbf{y}}$ direction), and Y is the $S\bar{S}$ pair center of mass. Due to the constraints imposed by the self-consistent-gap equation, two of the three configurational coordinates, R and K_0, are not independent;[35–37] we therefore consider the configurational coordinate defined by the product $s \equiv K_0 R$. The following equation defines the relationship between all configurational coordinates relevant to the $S\bar{S}$ intermediate state:

$$\tanh(K_0 R) \equiv \tanh(s) = K_0 \xi_0 = \frac{\xi_0}{\xi(R)} \equiv \bar{K}_0. \qquad (4)$$

As shown in Appendix D, the $S\bar{S}$ many-body electronic wave function $\Psi_{S\bar{S}}$ can be represented as a two-particle product constructed from various combinations of the upper and lower gap states; $\psi_{\pm\omega_0}$ are the one-electron parity eigenstates associated with the deformation in the bond alternation order parameter, which in turn are linear combinations of ψ_L and ψ_R, the left- and right-hand kink wave functions.[47] Note that the localization length of ψ_L and ψ_R, and therefore $\Psi_{S\bar{S}}$, depends on the $S\bar{S}$ separation $\xi(R) = \xi_0/\bar{K}_0$. The relationship between s, K_0, and R is shown in Fig. 1, and in Fig. 2 we plot the lattice order parameter and the corresponding self-localized $S\bar{S}$ electronic wave functions for several values of the configurational coordinate s, demonstrating the inverse relationship between the kink separation and the localization length of $\Psi_{S\bar{S}}$. For $s > 3$, the electron density becomes strongly localized on the left- and right-hand lattice kinks, eventually becoming two isolated and well-localized solitons. In the limit $s \Rightarrow 0$, the perfectly dimerized configuration, the $S\bar{S}$ electronic wave function extends over the entire lattice and merges with the valence and conduction band continuum at $\pm\Delta_0$.[37]

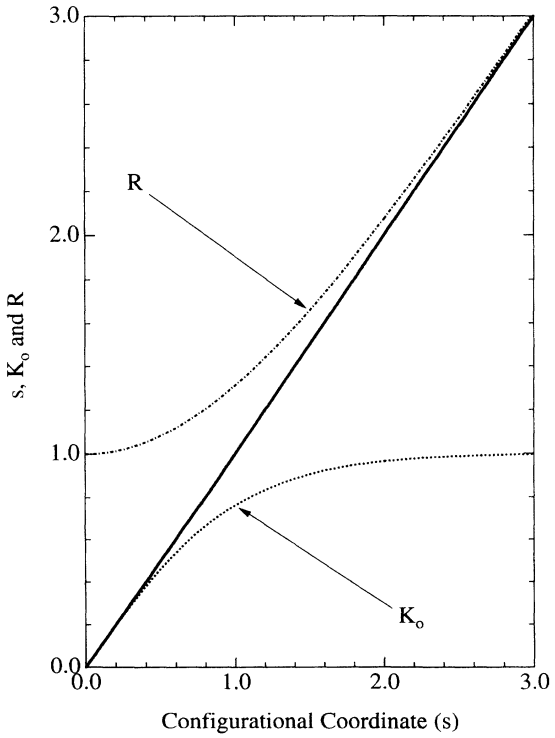

FIG. 1. The relationship between the configurational coordinates s, K_0, and R in units of the isolated kink coherence length ξ_0.

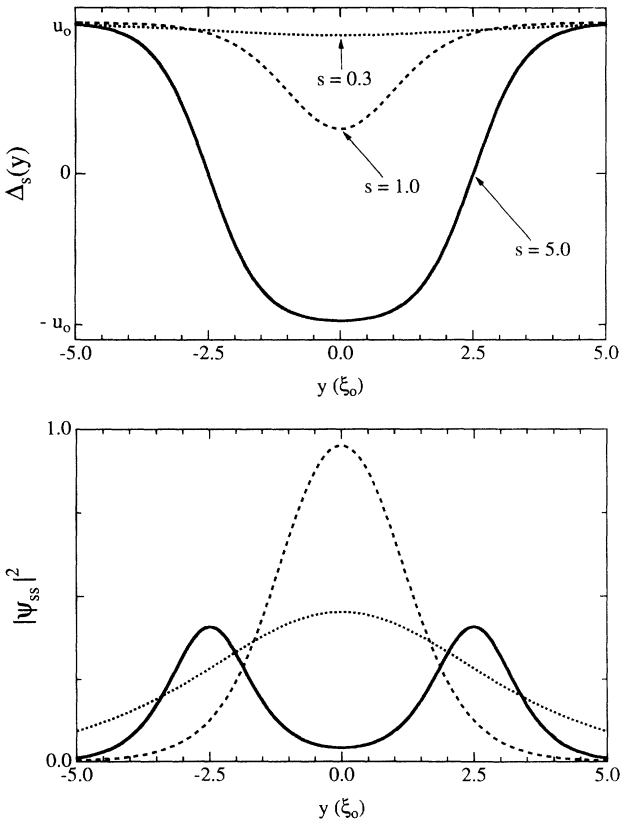

FIG. 2. Upper panel: the lattice order parameter in the continuum limit for three different values of the configurational coordinate s. Lower panel: the corresponding self-localized wave functions demonstrating the inverse relationship between the coherence length and the separation.

A. The $S\bar{S}$ electronic structure in the non-phase-shifted basis

To analyze the contribution of $S\bar{S}$ configurations to the optical susceptibility, we choose to define the electronic component of the wave function in the non-phase-shifted basis, i.e., the basis appropriate to the perfectly dimerized structure with translational symmetry. In this picture, as the two bond-alternation defects begin to separate, the electron-phonon interaction generates quantum mechanical coherence between individual Bloch orbitals resulting in the localized electronic structure of the $S\bar{S}$ electron-lattice configuration

$$|\Psi_{S\bar{S}}\rangle = \sum_k \sum_q |\psi_k^i \psi_q^j\rangle\langle\psi_k^i \psi_q^j|\Psi_{S\bar{S}}\rangle \quad (i,j = v,c). \qquad (5)$$

The independent sum over k and q reflects the two-

particle nature of the $S\bar{S}$ electronic wave function.[47] Note, however, that in the electric dipole approximation, momentum conservation requires that only the diagonal components of Eq. (5) couple to the external electromagnetic field.[40] The basis transformation defined in Eq. (5) is a mathematical convenience which allows us to calculate the optical properties of the infinite chain with an $S\bar{S}$ type excitation as a function of the separation s without having to rediagonalize the Hamiltonian.[37]

The diagonal component of the expansion coefficients appearing in Eq. (5) are defined in terms of an electronic enhancement factor I_0^2 times the $S\bar{S}$ spectral density function $G(s,k)$, which defines the spectral decomposition of the projection of the $S\bar{S}$ electronic state onto the non-phase-shifted basis

$$\langle \psi_k^i \psi_k^j | \Psi_{S\bar{S}} \rangle \propto \beta(s,k) = \frac{1}{N} \left(\frac{\pi^2}{2} \frac{\xi_0}{a} \right) \frac{1}{\bar{K}_0} \mathrm{sech}^2 \left(\frac{\pi}{2} \frac{k\xi_0}{\bar{K}_0} \right) \equiv \frac{1}{N} I_0^2 G(s,k). \quad (6)$$

The large magnitude of the electronic enhancement factor $I_0^2 \approx 35$ is a result of the delocalized nature of the $S\bar{S}$ wave function as compared to the Wannier functions of the rigid lattice, which have a spatial extent on the order of the unit cell.[48,49] Note that in the Bloch representation the isolated soliton wave function is localized as the Bloch wave functions extend over the entire lattice. The magnitude of I_0^2 was confirmed by Feldblum *et al.*[50] in detailed quantitative *in situ* doping studies on *trans*-$(CH)_x$.

B. The $S\bar{S}$ localization length and spectral density function

In this section, we illustrate an important relationship between the $S\bar{S}$ separation, the coherence length, and the quantity of the oscillator strength (virtual or real) transferred from the valence and conduction band continuum to the $S\bar{S}$ electron-lattice configuration. The two-particle mixed-basis formalism [Eqs. (5) and (6)], with a minor empirical mass correction,[51] is found to conserve the π-electron oscillator strength for all values of the $S\bar{S}$ separation and demonstrates that the largest shifts of oscillator strength occur for a well-separated $S\bar{S}$ pair. We emphasize that oscillator strength conservation forms the basis for the $S\bar{S}$ intermediate state mechanism which dominates the third-order nonlinear susceptibility as described below in Sec. VII B.

We define $L_{S\bar{S}}$ to be the localization length of the $S\bar{S}$ electron-lattice configuration; for $s < 3$, $L_{S\bar{S}}$ is approximately the length over which the $S\bar{S}$ electronic wave function is extended along the chain[36]

$$L_{S\bar{S}} = R + 2\,\xi(R) = \xi_0\,(s+2)/\bar{K}_0. \quad (7)$$

It is clear from Eq. (4) and Figs. 1 and 2 that the minimum separation is $R = \xi_0$, at which point the coherence length $\xi(R)$ becomes infinite, with the $S\bar{S}$ electron-lattice configuration delocalized over the entire chain

$$\lim_{s\to 0} L_{S\bar{S}} = \xi_0 + 2\,\frac{1}{2}(Na - \xi_0) = Na = L. \quad (8)$$

In this limit, the projection of the $S\bar{S}$ electronic wave function onto the non-phase-shifted basis becomes quasimonochromatic and eventually merges with the valence and conduction band continuum at $\pm\Delta_0$:[37]

$$\lim_{s\to 0} G(s,k) = \frac{2}{\pi}\,\delta(k). \quad (9)$$

Hence there is no phonon-assisted transfer of oscillator strength from the valence and conduction band continuum to the midgap levels; the system is in the rigid-lattice configuration.

As shown in Fig. 2, for $s > 3$, the electron density becomes strongly localized on the left- and right-hand solitons. To illustrate the electronic structure of the well-separated $S\bar{S}$ pair in the non-phase-shifted basis, recall that for a spatial δ function the projection amplitude is uniform in the Bloch wave vector k, i.e., $\sum_k e^{ik\cdot R} = \delta(R)$. This is simply the equivalence of the Bloch and Wannier descriptions of the electronic states in the noninteracting rigid lattice.[38] The isolated soliton wave functions, on the other hand, have a intermediate localization length $L/a \gg \xi_0/a \gg 1$; therefore the expan-

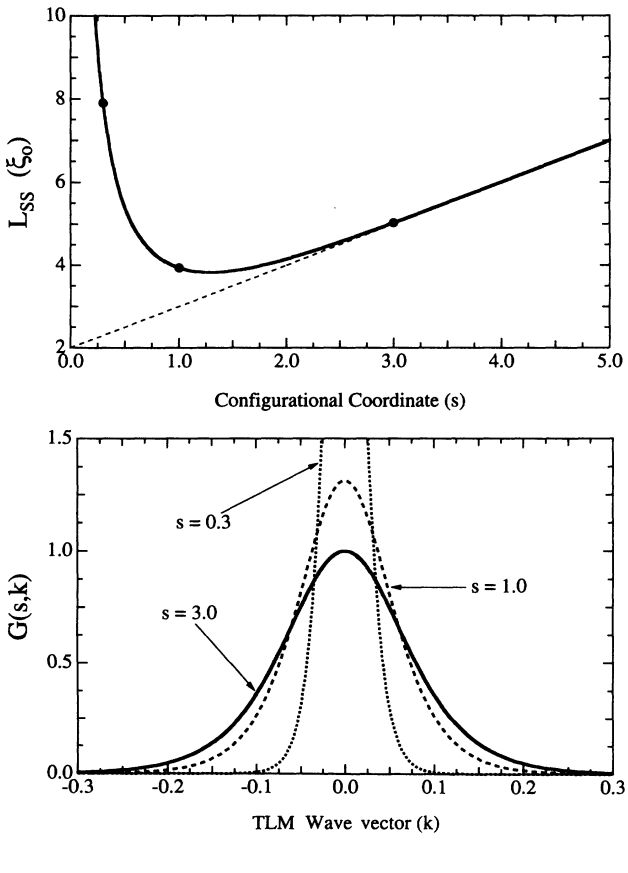

FIG. 3. Upper panel: the $S\bar{S}$ localization length, Eq. (7), as a function of the $S\bar{S}$ separation, demonstrating that for small s, the $S\bar{S}$ wave function is highly delocalized. The dashed line is $y = \xi_0(s+2)$ and corresponds to the linear separation of two well-localized solitons. Lower panel: the spectral density removed from the valence and conduction continuum by the gap-state wave functions. As the soliton-antisoliton separation s decreases, the distribution approaches a δ function at $\pm\Delta_0$ [see Eq. (9)].

sion is never uniform in k but rather reflects the Fourier transformation properties of the soliton wave function [see Eq. (B1)]

$$\lim_{s\to\infty} G(s,k) = \mathrm{sech}^2\left(\frac{\pi}{2}k\xi_0\right). \tag{10}$$

Hence, for large separation the projection of the $S\bar{S}$ electronic wave function onto the eigenstates of the non-phase-shifted basis remains peaked at $\pm\Delta_0$, but extends well into the band.

The localization length $L_{S\bar{S}}$ is plotted in the upper panel of Fig. 3 as a function of the $S\bar{S}$ separation. In the lower panel, the $S\bar{S}$ spectral density function $G(s,k)$ projecting a single $S\bar{S}$ pair onto the non-phase-shifted basis is plotted for several values of the separation s. It is clear that for a well-separated $S\bar{S}$ pair, large shifts of π-electron oscillator strength are required to construct the localized $S\bar{S}$ electronic wave function. Note that as the soliton-antisoliton separation decreases, the $S\bar{S}$ localization length increases and the $S\bar{S}$ spectral density function becomes more strongly peaked at $\pm\Delta_0$; eventually $G(s,k)$ becomes a δ function centered at the band edge and $L_{S\bar{S}}$ spans the entire chain. As shown in Sec. V A, these complementary trends require that the effective density of $S\bar{S}$ pairs on the infinite chain be a function of the $S\bar{S}$ separation. The relationship between $L_{S\bar{S}}$, $G(s,k)$, and the effective density of $S\bar{S}$ pairs is an essential statement of oscillator strength conservation for the system with nonlinear zero-point motion.

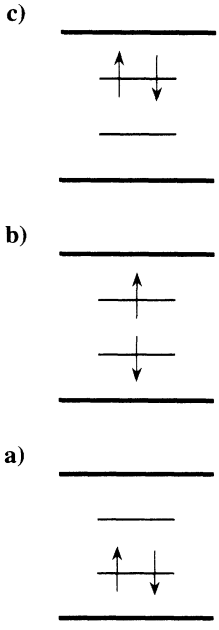

FIG. 4. The gap-state energy level diagram showing the occupancies corresponding to the three $S\bar{S}$ two-particle singlet electronic configurations. Configuration (a) is the A_g symmetric ground state, configuration (b) is the B_u symmetric charged $S\bar{S}$ pair, and configuration (c) is the A_g symmetric neutral $S\bar{S}$ pair.

C. Total energy and symmetry of the $S\bar{S}$ electron-lattice configuration

The total energy (electronic and lattice) of the $S\bar{S}$ electron-lattice configuration is a function of the relative occupation of $\psi_{\pm\omega_0}$ and the separation $s = K_0R$ of the $S\bar{S}$ pair:[36]

$$E^{\nu}_{S\bar{S}} = \frac{4\Delta_0}{\pi}\{\tanh(s) + \cos^{-1}[\tanh(s)]\mathrm{sech}(s)\} + (n_+ - n_-)\,\Delta_0\,\mathrm{sech}(s), \tag{11}$$

where n_+ and n_- are the respective occupation numbers of $\psi_{\pm\omega_0}$ and $2\Delta_0$ is the $\pi-\pi^*$ energy gap.[42] Charge neutrality of the photoexcited chain requires that the midgap states associated with the $S\bar{S}$ pair are occupied by two electrons. Since there are two single-particle levels associated with the $S\bar{S}$ pair, there are three distinct two-particle singlet electronic configurations defined by the relative occupations of $\psi_{\pm\omega_0}$, $\nu \equiv (n_+ - n_-) = -2, 0, 2$, shown schematically in Fig. 4. Because polyacetylene is a member of the C_{2h} symmetry group, these $S\bar{S}$ electron-lattice configurations have either A_g or B_u symmetry.[52]

The configurational potential energy surfaces generated by Eq. (11) are shown in Fig. 5 for the occupations of the midgap levels depicted in Fig. 4, demon-

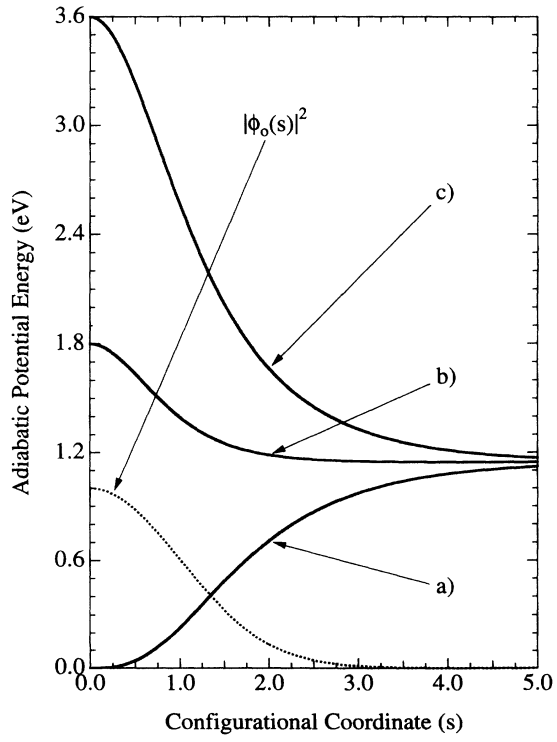

FIG. 5. Configurational potential energy diagrams corresponding to the gap-state occupancies depicted in Fig. 4. Curve a is the A_g symmetric ground state, curve b is the B_u symmetric charged $S\bar{S}$ pair that evolves from a free electron-hole pair, and curve c is the neutral $S\bar{S}$ pair that evolves from the $2A_g$ state in the noninteracting rigid lattice. Also shown is $|\phi_0(s)|^2$, the ground state $S\bar{S}$ probability distribution, Eq. (17).

strating that, for finite separation, the creation energy of the $S\bar{S}$ pair is less than the classical energy gap. In the limit of large separation, the energy of the $S\bar{S}$ configuration is $E_{S\bar{S}} \Rightarrow 4\Delta_0/\pi$ independent of the occupation; the three electronic configurations become energetically degenerate. Wu and Kivelson have shown, however, that this degeneracy is lifted by even weak electron-electron interactions.[53,54] Nevertheless, the energy of the well-separated $S\bar{S}$ electron-lattice configuration is significantly lower than the one- and two-photon energy gaps, $2\Delta_0$ and $4\Delta_0$, respectively, of the noninteracting rigid lattice. The subgap energy of the $S\bar{S}$ electron-lattice configuration in conjunction with the localization of the $S\bar{S}$ electronic wave function, which requires the weighted coherent summation of momentum eigenstates with energies equal to, or greater than, $2\Delta_0$ for single-photon excitations or $4\Delta_0$ for the two-photon excitations, implies that large shifts of oscillator strength are associated with $S\bar{S}$ type excitations.

Since the continuum of soliton-antisoliton electron-lattice configurations falls below the energy of the interband $\pi-\pi^*$ transition in a rigid-lattice model, one might anticipate that soliton pairs could be directly photogenerated at energies below the band edge, i.e., within the continuum from $4\Delta_0/\pi \leq \hbar\omega \leq 2\Delta_0$. Indeed, since the charged soliton pair evolves continuously from an excited electron-hole pair,[27] there is an $S\bar{S}$ configuration with B_u symmetry.[47] Therefore, an electric dipole moment matrix element from the ground state (with A_g symmetry) to a B_u symmetric $S\bar{S}$ electron-lattice configuration does exist. In order for the transition to be allowed, however, there must be a finite overlap between the ground and excited state lattice wave function as well. The lattice overlap between the ground state and the $S\bar{S}$ electron-lattice excited state is considered in the following section.

IV. THE NONLINEAR FRANCK-CONDON FACTOR

The Born-Oppenheimer approximation

We assume that the many-body wave function of the $S\bar{S}$ electron-lattice configuration is given by the Born-Oppenheimer product

$$|S\bar{S}\rangle = |\Psi_{S\bar{S}}(s)\rangle \otimes |\Phi_{\mathrm{ex}}(s,Y)\rangle, \tag{12}$$

where $|\Psi_{S\bar{S}}(s)\rangle$ and $|\Phi_{\mathrm{ex}}(s,Y)\rangle$ are, respectively, the many-body electronic and lattice wave functions corresponding to a single $S\bar{S}$ pair with separation s and center of mass coordinate Y. The ground state of the coupled electron-phonon system is given by

$$|G\rangle = |g\rangle \otimes |\Phi_0\rangle, \tag{13}$$

where $|g\rangle$ is the many-body electronic wave function of the ground state and $|\Phi_0\rangle$ is the ground state lattice wave function. Hence the matrix elements become the product of an electronic matrix element and a Franck-Condon lattice overlap factor

$$\langle S\bar{S}|\mathbf{y}|G\rangle = \langle \Psi_{S\bar{S}}(s')|\mathbf{y}|g\rangle \otimes \langle \Phi_{\mathrm{ex}}(s')|\Phi_0\rangle, \tag{14}$$

where, for instance, $\langle \Psi_{S\bar{S}}(s)|\mathbf{y}|g\rangle$ denotes the electronic dipole matrix element between the ground and $S\bar{S}$ excited state electronic wave functions and $\langle \Phi_{\mathrm{ex}}(s,Y)|\Phi_0\rangle$ is the overlap between the ground and $S\bar{S}$ excited state lattice wave functions.

As is well known in optical studies of the finite polyenes[55] and nondegenerate-ground-state polymers,[18,23] the quantum mechanical zero-point motion of the lattice allows direct access to the electronic states of the relaxed configuration, resulting in the Franck-Condon vibronic progressions observed in both the absorption and emission spectra. In *trans*-$(CH)_x$, where the potential energy surfaces are anharmonic (see Fig. 5), nonlinear zero-point motion allows direct access to excited electronic states associated with $S\bar{S}$ lattice configurations.[28–32] In order to evaluate Eq. (14), one must determine both the ground and excited state lattice wave functions.

In *trans*-$(CH)_x$ the excited state configurational potential energy surface is unbounded and may therefore be treated classically with every s corresponding to a different electronic eigenstate. In this semiclassical approximation, the Franck-Condon overlap between the ground state and the excited state $S\bar{S}$ continuum is simply the ground state probability amplitude evaluated at the excited state lattice configuration s',[32]

$$\langle \Phi_{\mathrm{ex}}(s')|\Phi_0\rangle = |\Phi_0(s')|. \tag{15}$$

V. THE MODEL GROUND STATE LATTICE WAVE FUNCTION

Monte Carlo calculations have demonstrated that quantum lattice fluctuations significantly modify the electronic density of states by reducing the amplitude of the zero-temperature dimerization.[56–59] These simulations show much structure in the instantaneous lattice configuration for degenerate-ground-state conjugated polymers, demonstrating both harmonic and long-wavelength anharmonic contributions. Since the high-frequency harmonic terms, which yield simple Franck-Condon vibronic progressions, tend to average out, the observed reduction in the classical dimerization is primarily a result of low-frequency long-wavelength anharmonic quantum lattice fluctuations. In the model presented here, the reduction in the dimerization and the corresponding modifications imparted to the electronic density of states are the result of an as yet unspecified effective density $\rho_s \equiv N_s/N$ of $S\bar{S}$ pairs in the ground state.

As a first approximation, we adopt the following model for the anharmonic component of the ground-state lattice wave function.

(i) The ground state lattice wave function is described as a statistical distribution of instantaneous lattice configurations describing N_s identical noninteracting $S\bar{S}$ pairs of separation s, each located at an arbitrary center of mass coordinate Y_i.

(ii) The total number of $S\bar{S}$ pairs in a given instantaneous lattice configuration is limited by the constraint that the sum of the expansion coefficients projecting the

N_s self-localized $S\bar{S}$ electronic wave functions onto a given momentum eigenstate of the completely delocalized non-phase-shifted basis must be less than unity.

(iii) The effective density of $S\bar{S}$ pairs in the ground state $\rho_s = N_s/N$ is determined such that the total dimerization amplitude is reduced by 10–20 %, consistent with the Monte-Carlo calculations presented in Refs. 56–59.

We assume, therefore, that the zero-point motion of the lattice can be modeled in terms of the following instantaneous lattice configurations:

$$|\Phi_0(s)\rangle = \prod_{i=1}^{N_s(s)} |\phi_0(s,Y_i)\rangle = |\phi_0(s)\rangle \prod_{i=1}^{N_s(s)} \delta(Y_i), \quad (16)$$

where the product is over the $N_s(s)$ center of mass coordinates and $|\phi_0(s)|^2$ denotes the ground state probability distribution for finding a given $S\bar{S}$ pair with separation s at arbitrary center of mass coordinate Y_i,[60]

$$|\phi_0(s)|^2 = \frac{1}{\sqrt{2\pi}} \exp\left(-\frac{1}{2}\, s^2\right). \quad (17)$$

The total ground state lattice wave function is given by the weighted sum over all instantaneous lattice configurations

$$|\Phi_0\rangle = \sum_s |\Phi_0(s)\rangle = \sum_s |\phi_0(s)\rangle \prod_{i=1}^{N_s(s)} \delta(Y_i). \quad (18)$$

In this approximation, all the $S\bar{S}$ pairs in a given instantaneous lattice configuration have the same separation; i.e., the instantaneous lattice configuration is completely specified by the configurational coordinate s. The individual $S\bar{S}$ pairs are distinguished by their arbitrary center of mass coordinate. The factor $N_s(s)$ which appears below in the $S\bar{S}$ contribution to the linear and nonlinear optical susceptibility is a result of the sum over all-excited states and reflects the energetic degeneracy of the $N_s(s)$ distinct and noninteracting $S\bar{S}$ electronic configurations contributing to a given linear or nonlinear process.

The effective density of $S\bar{S}$ pairs in the ground state lattice wave function

The expansion coefficients projecting N_s identical noninteracting $S\bar{S}$ electron-lattice configurations onto the non-phase-shifted basis are obtained by simply multiplying $\beta(s,k)$ by N_s. Since the non-phase-shifted valence and conduction band continuum form a complete basis, the sum of the expansion coefficients projecting the N_s $S\bar{S}$ electronic wave functions onto a given Bloch eigenstate of the non-phase-shifted basis must be less than unity; i.e., for any Bloch wave vector k, $N_s\beta(s,k) \leq 1$. This constraint implies that there is an upper limit to the number of $S\bar{S}$ configurations that can be supported by the chain and that this number depends on the separation s of the noninteracting $S\bar{S}$ pairs; as the separation s decreases, the coherence length of the individual $S\bar{S}$ wave functions increases and the projection onto the non-phase-shifted basis $G(s,k)$ approaches a δ function at $\pm\Delta_0$ (see Figs. 2 and 3). The system is therefore able to support fewer and fewer $S\bar{S}$ pairs due to a depletion of the spectral density at the band edge; i.e., the intensity of the Bloch states at $\pm\Delta_0$ is exhausted by the projection. Therefore, as s decreases, the number of $S\bar{S}$ pairs must decrease, and in particular as $s \Rightarrow 0$, the total number of $S\bar{S}$ pairs on a given polyacetylene chain is at most one.

To get a reduction in Δ_0 therefore requires that the number of identical $S\bar{S}$ pairs in the array must be an increasing function of the $S\bar{S}$ separation s. Equation (6) states that the number of identical $S\bar{S}$ pairs must be inversely proportional to the coherence length; $N_s \Rightarrow N_s(s) = N_s^0 \bar{K}_0$, where N_s^0 is the effective number of $S\bar{S}$ pairs in the ground state and $\bar{K}_0 = \xi_0/\xi(R)$. This is the origin of the excluded volume factor $\bar{K}_0$, appearing below in Eq. (19) and in the expressions for the $S\bar{S}$ contribution to the linear and third-order nonlinear optical susceptibility. The phase-space-filling–excluded-volume constraint also places a maximum on the density of well separated $S\bar{S}$ pairs; $\rho_s^{\max} \equiv I_0^{-2} = 2a/\pi^2\xi_0 = 2.9\%$,

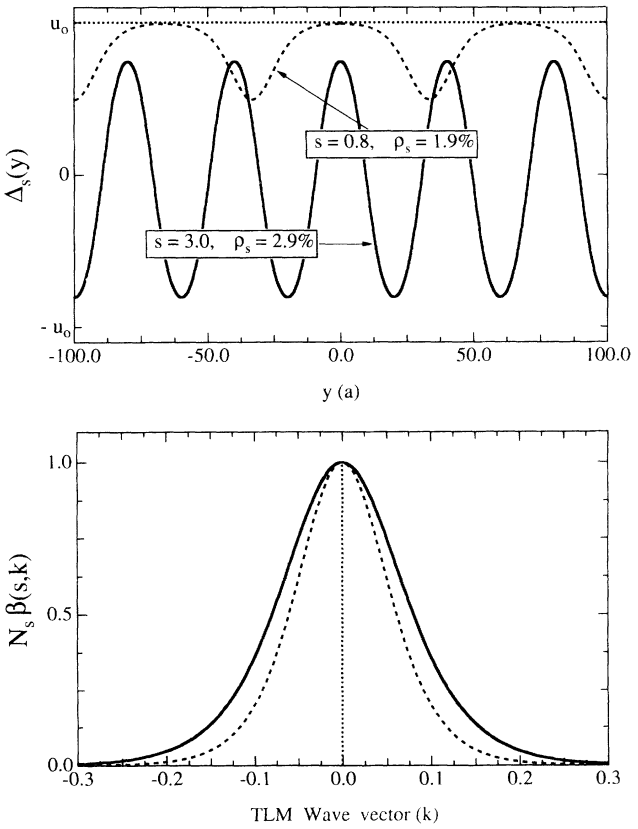

FIG. 6. Upper panel: the instantaneous lattice configuration of a 200 site chain for three values of the configurational coordinate s. The horizontal line (dotted) at the top of the figure corresponds to the perfectly dimerized configuration: $s = 0$, $\rho_s = 1/N$. Note the inverse relationship between the $S\bar{S}$ coherence length and the number density. The ground state lattice wave function is obtained by weighting the instantaneous lattice configurations by $\phi_0(s)$. Lower panel: the corresponding expansion coefficients projecting the $N_s(s) = N_s^{\max}\, \bar{K}_0$ $S\bar{S}$ electron-lattice configurations onto the non-phase-shifted basis. The projection of the perfectly dimerized configuration is a δ function centered at the band edge (dotted vertical line).

above which the $\pi - \pi^*$ interband transition at $2\Delta_0$ is completely depleted. It is interesting to note that this density of $S\bar{S}$ pairs is precisely the concentration at which a metal-insulator phase transition is observed in doping studies on *trans*-polyacetylene.[61,62]

From the 10–20% reduction in the magnitude of the bond alternation (compared with that in the classical lattice approximation) due to nonlinear zero-point motion,[56–59] one can estimate the effective density of $S\bar{S}$ pairs in the ground state $\rho_s^0 = N_s^0/N$:

$$(0.10-0.20)\Delta_0 = \rho_s^0 \iint dy\, ds\, \bar{K}_0\,[\Delta_s(y)-\Delta_0]\,|\phi_0(s)|^2, \tag{19}$$

where $\Delta_s(y)$ is the site dependent order parameter in the presence of an $S\bar{S}$ pair with separation s as described in Eq. (3). From Eq. (19), one finds $\rho_s^0 \approx 2.5\% \leq \rho_s^{\max}$. Equation (19) ensures that the model ground state lattice wave function is consistent with the results of the Monte Carlo calculations.[56–59] The instantaneous lattice configuration is plotted in the upper panel of Fig. 6 for several values of the separation s, demonstrating the inverse relationship between the $S\bar{S}$ coherence length and the number density. The lower panel shows the expansion coefficients projecting the $\rho_s(s) = \rho_s^{\max}\bar{K}_0$ identical, noninteracting $S\bar{S}$ electronic wave functions onto the non-phase-shifted basis.

VI. THE SSH LINEAR SUSCEPTIBILITY

A number of different approaches to calculating the contribution of direct photoproduction of charged solitons to $\chi^{(1)}(\omega)$ have appeared in the literature.[28–32] The problem is of interest because this contribution to $\chi^{(1)}(\omega)$ would not exist for a classical lattice. The subgap direct photoproduction of charged soliton pairs relies on quantum lattice fluctuations; without such nonlinear zero-point motion there would be no overlap of the lattice wave function of the perfectly dimerized ground state with that of the chain containing a kink-antikink pair. The linear susceptibility calculation therefore provides a reasonable test of the accuracy with which we treat the nonlinear Franck-Condon factor.

A. Rigid-lattice contribution

The contribution to the linear term in the dielectric (optical) susceptibility from interband $\pi - \pi^*$ transitions in a noninteracting rigid lattice has been calculated in detail previously.[42,49] We outline the calculation here because we want to compare the rigid-lattice result with that calculated for the infinite chain with nonlinear zero-point motion. As shown in Sec. II, the rigid-lattice limit of the SSH linear susceptibility as obtained from first-order time dependent perturbation theory is given by

$$\chi_{\rm RL}^{(1)}(\omega) = e^2\,\frac{1}{V}\sum_k \langle G|\mathbf{y}|K_I\rangle\langle K_I|\mathbf{y}|G\rangle \times\left[\frac{1}{[E_{cv}(k)-\omega]}+\frac{1}{[E_{cv}^*(k)+\omega]}\right], \tag{20}$$

where the sum is over all vertical transitions and $V = Na/\sigma$ is the volume occupied by a single polyacetylene chain; i.e., $\mathbf{P}(\omega) = \chi^{(1)}(\omega)\mathbf{E}(\omega)$ is the dipole moment per unit volume and $\mathbf{E}(\omega)$ is the macroscopic electric field; in this analysis local-field effects are not considered. Our strategy is to express the linear susceptibility in terms of a constant prefactor times a dimensionless integral of order unity. For this purpose, we define the following dimensionless energy variables: $x = [E_{cv}(k) - i\Gamma_k/2]/2\Delta_0$ and $z = \hbar\omega/2\Delta_0$, and convert the sum over k to an integral weighted by the joint density of electronic states[63]

$$\begin{aligned}\sum_k &\Rightarrow 2\,\frac{Na}{2\pi}\int_0^{\pi/2a} dk \\ &= 2\,\frac{Na}{2\pi}\,2\Delta_0\int_1^{W/2\Delta_0} dx\;\rho_{cv}(x) \\ &= \frac{Na}{\pi\xi_0}\int_0^{\pi\xi_0/2a} dZ = \frac{N}{2}.\end{aligned} \tag{21}$$

The joint density of electronic states and the dipole moment matrix elements are discussed in detail in Appendixes E and F, respectively. The linear susceptibility can now be written as a numerical prefactor times a dimensionless integral containing the band-edge square-root singular resonance at $2\Delta_0$:

$$\chi_{\rm RL}^{(1)}(z) = |\chi_0^{(1)}|_{\rm RL}\int dZ\,\frac{1}{|x|^3}\,\frac{1}{(x-z)(x^*+z)}. \tag{22}$$

The rigid-lattice linear susceptibility prefactor is given by

$$|\chi_0^{(1)}|_{\rm RL} = 4\frac{1}{\pi}\,e^2\,(f_{cv}^0)^2\,\sigma\,\rho_{cv}^0 \;\approx 1.9\ \text{esu}, \tag{23}$$

where $\sigma = L/V$, and f_{cv}^0 and ρ_{cv}^0 are the prefactors for the π-electron dipole moment matrix elements and the joint density of states, respectively (see Appendix H).

B. B_u symmetric $S\bar{S}$ contribution

The contribution of the $S\bar{S}$ continuum to the linear susceptibility is given by

$$\chi_{S\bar{S}}^{(1)}(\omega) = e^2\,\frac{1}{V}\sum_s N_s(s)\,\langle G|\mathbf{y}|S\bar{S}\rangle\langle S\bar{S}|\mathbf{y}|G\rangle \times\left[\frac{1}{(E_{S\bar{S}}^{\nu}-\omega)}+\frac{1}{(E_{S\bar{S}}^{\nu *}+\omega)}\right], \tag{24}$$

where the $S\bar{S}$ electronic configurations are defined in Appendix D. The factor $N_s(s)$ appearing in Eq. (24) results from the ground state lattice wave function being able to support (statistically) $N_s(s)$ noninteracting, incoherent and energetically degenerate $S\bar{S}$ electronic configurations, as described in detail in Sec. V. Converting the sum over the $S\bar{S}$ separation to an integral yields

$$\chi_{S\bar{S}}^{(1)}(z) = 2e^2\frac{1}{V}\frac{1}{2\Delta_0}\int_0^{\infty} ds N_s(s)\langle G|\mathbf{y}|S\bar{S}\rangle\langle S\bar{S}|\mathbf{y}|G\rangle \times\frac{|w_\nu|}{(w_\nu - z)(w_\nu^* + z)} \tag{25}$$

where $w_\nu = (E_{S\bar{S}}^{\nu} - i\Gamma_s^{\nu}/2)/2\Delta_0$ is the dimensionless $S\bar{S}$

energy variable.

As shown in Fig. 4, for a given $S\bar{S}$ lattice configuration, there are three distinct singlet $S\bar{S}$ electronic states, defined by the relative occupation of the upper and lower gap states ν. Of these, two have A_g symmetry and one has B_u symmetry. Since the many-body ground state has A_g symmetry, it has a nonvanishing dipole matrix element only to that configuration with B_u symmetry. The potential energy surface corresponding to the A_g symmetric ground state and the B_u symmetric first excited state along with the ground state lattice wave function describing the nonlinear zero-point motion are shown in Fig. 5.

To calculate the dipole moment matrix element, we expand the $S\bar{S}$ many-body electronic wave function in the non-phase-shifted basis and sum the individual interband rigid lattice momentum matrix elements weighted by the appropriate expansion coefficient. The electronic matrix element connecting the ground state to the B_u symmetric $S\bar{S}$ configuration is shown in Appendix G to be given by

$$\langle g|\mathbf{y}|\Psi^{\pm}_{S\bar{S}}\rangle = \sqrt{2}\,\frac{\pi}{2}\,f^0_{cv}\,\Sigma_{\pm}(s), \tag{26}$$

where

$$\Sigma_{\pm}(s) \equiv \frac{1}{|w_0|}\int dZ\,\frac{1}{|x|}\,G(s,x) \tag{27}$$

is the Fourier decomposition of the electronic dipole moment matrix element between the many-body ground state and a single B_u symmetric $S\bar{S}$ electron-lattice configuration of separation s; $I_0^2\,G(s,x)/N$ is the expansion coefficient projecting the dipole moment of a single B_u symmetric $S\bar{S}$ configuration onto the non-phase-shifted basis.

The $S\bar{S}$ contribution to the linear optical susceptibility can be written, therefore, as

$$\chi^{(1)}_{S\bar{S}}(z) = |\chi^{(1)}_0|_{S\bar{S}}\int ds\;\bar{K}_0\,\frac{|w_0|}{(w_0+z)(w_0^*-z)} \times |\phi_0(s)|^2\,\Sigma^2_{\pm}(s), \tag{28}$$

with the $S\bar{S}$ linear susceptibility prefactor given by

$$|\chi^{(1)}_0|_{S\bar{S}} = \rho_s^0 4\,e^2\,\left(\frac{\pi}{2}\,f^0_{cv}\right)^2\frac{\sigma}{a}\,\frac{1}{2\Delta_0} = \rho_s^0 - 110\ \text{esu}. \tag{29}$$

The ratio of the $S\bar{S}$ and rigid-lattice linear susceptibility prefactors is given by the following expression:

$$\frac{|\chi^{(1)}_0|_{S\bar{S}}}{|\chi^{(1)}_0|_{\mathrm{RL}}} = \rho_s^0 \times \frac{\pi}{2}\,I_0^2, \tag{30}$$

which, as expected, is proportional to both the electronic enhancement factor and the effective density of $S\bar{S}$ pairs in the ground state. For $\rho_s^0 = \rho_s^{\max}$ this ratio is $\pi/2$, which is the ratio of the non-phase-shifted band gap to the creation energy of a well-separated $S\bar{S}$ pair, i.e., $\pi/2 = 2\Delta_0/(4\Delta_0/\pi)$.

C. Total linear susceptibility

Since the electronic structure of the rigid lattice and that of the lattice containing an $S\bar{S}$ type configuration are related by a simple basis transformation, the total $\pi-\pi^*$ oscillator strength must be conserved. Hence $\chi^{(1)}(\omega)$ must satisfy the oscillator strength sum rule:[63]

$$\int d\omega\;\omega\;\mathrm{Im}\{\chi^{(1)}(\omega)\} = \frac{1}{8}\,\Omega_p^2, \tag{31}$$

where Ω_p is the plasma frequency, $\Omega_p^2 = 4\pi n e^2/m_e$, and $n = N/V$ is the density of π electrons with charge e and mass m_e. In the rigid-lattice limit the oscillator strength sum rule is exhausted by all excitations involving free electron-hole pairs. As a result, any oscillator strength associated with the direct photoproduction of charged solitons must be acquired at the expense of the rigid-lattice contribution. This transfer of oscillator strength is analogous to that which occurs when the polymer is doped; the doping-induced oscillator strength near midgap is transferred from the total $\pi-\pi^*$ transition, resulting in a bleach of the interband absorption and the appearance of optically allowed transitions within the classically forbidden energy gap.[42] Hence, in order to conserve total oscillator strength, Eq. (20) must be modified to account for the spectral density present in the coherent superposition comprising the gap-state wave functions [see Eq. (5)]. We therefore write the total linear susceptibility as

$$\chi^{(1)}(\omega) = \chi^{(1)}_0 + \chi^{(1)}_{S\bar{S}}(\omega;\rho_s^0) + \chi^{(1)}_{\mathrm{RL}}(\omega;\rho_s^0), \tag{32}$$

where $\chi^{(1)}_0$ is the dc offset resulting from excitations involving the higher energy σ and core electrons. The rigid-lattice contribution is now given by

$$\chi^{(1)}_{\mathrm{RL}}(z;\rho_s^0) = |\chi^{(1)}_0|_{\mathrm{RL}}\int ds\;|\phi_0(s)|^2\int dZ\,\frac{1}{|x|^3}\,\frac{1}{(x+z)(x^*-z)} \times[1-N_s(s)\beta(s,x)]. \tag{33}$$

The second term on the right-hand side in Eq. (33) self-consistently corrects the rigid-lattice contribution to the linear susceptibility for the oscillator strength transferred out of the vertical interband transition and into transitions involving the direct photoproduction of $N_s(s)$ identical, noninteracting B_u symmetric (charged) $S\bar{S}$ electronic configurations; $\beta(s,x) = I_0^2\,G(s,x)/N$ is the $S\bar{S}$ interband spectral density function, which measures the total oscillator strength transferred out of the vertical interband transition and into transitions involving the direct photoproduction of a single B_u symmetric $S\bar{S}$ electronic configuration for optical energy between x and $x+dx$.

The total linear susceptibility for the rigid lattice, Eq. (22), and the infinite chain with nonlinear zero-point motion, Eq. (32), have been evaluated numerically using the parameters listed in Appendix H and assuming $\rho_s^0 \Rightarrow \rho_s^{\max}$. The results for the real and imaginary components of $\chi^{(1)}(\omega)$ are plotted in Figs. 7 and 8, respectively, demonstrating that the inclusion of nonlinear zero-point motion leads to a large shift of oscillator strength from the electron-hole pair continuum to states below

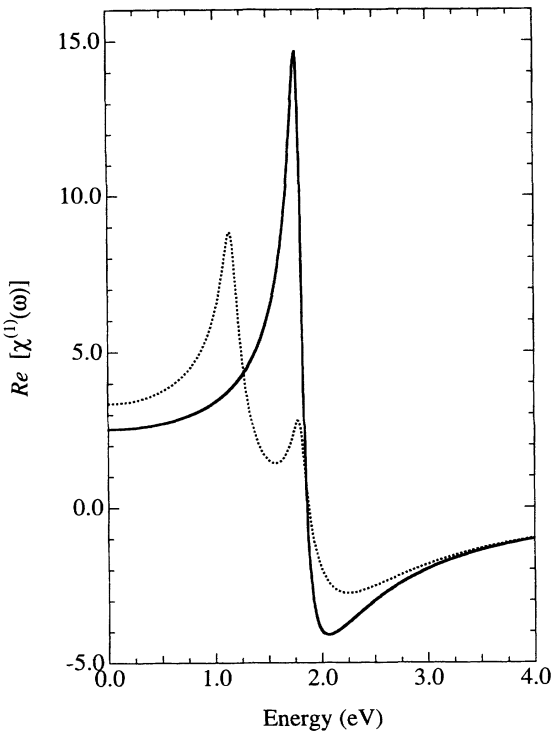

FIG. 7. The real part of the SSH linear susceptibility in the rigid-lattice approximation (bold) and with the inclusion of nonlinear zero-point motion (dotted).

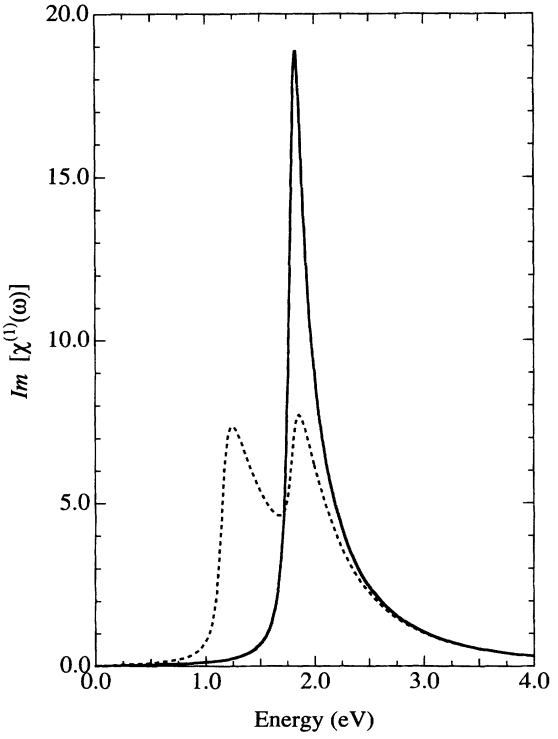

FIG. 8. The imaginary part of the SSH linear susceptibility in the rigid-lattice approximation (bold) and with the inclusion of nonlinear zero-point motion (dotted). The low-energy feature which appears upon the inclusion of the nonlinear zero-point motion corresponds to the direct photoproduction of charged soliton pairs.

the classical energy gap. The feature which appears on the low energy side of the spectrum corresponds to the direct photoproduction of charged solitons and is spectrally consistent with the measured photoconductivity action spectrum.[16,17] The π-electron integrated oscillator strength, Eq. (31), is shown in Fig. 9, demonstrating that the oscillator strength sum rule is properly satisfied for both the rigid lattice and the infinite chain with nonlinear zero-point motion;[51] for both contributions we find $\Omega_p \approx W \equiv 2\Delta_0(\xi_0/a)$.

D. Experimental comparison

The absorption coefficients $\alpha(\omega) = 2\omega\kappa(\omega)/c$, calculated from $\chi^{(1)}(\omega)$,[63] for the rigid-lattice and the infinite chain with nonlinear zero-point motion are compared in Fig. 10. The agreement of the latter with experiment is satisfactory; the magnitude and overall shape of $\alpha(\omega)$ are in general agreement with measurements on oriented *trans*-$(CH)_x$.[20,26]

The shoulder on the leading edge of the absorption curve is a general feature of *trans*-$(CH)_x$, and while it is observable in both the absorption spectra[19,22] and the photoconductivity action spectrum[16,17] of nonoriented samples, it is more clearly visible in data obtained from oriented samples; it is seen directly in the absorption spectrum[26] and in the *measured* reflectivity spectrum (see Fig. 1 in Ref. 20). Using polarized electroabsorption spectroscopy, Phillips *et al.*[22] demonstrated that, in the oriented material, this "low-energy" feature, which follows

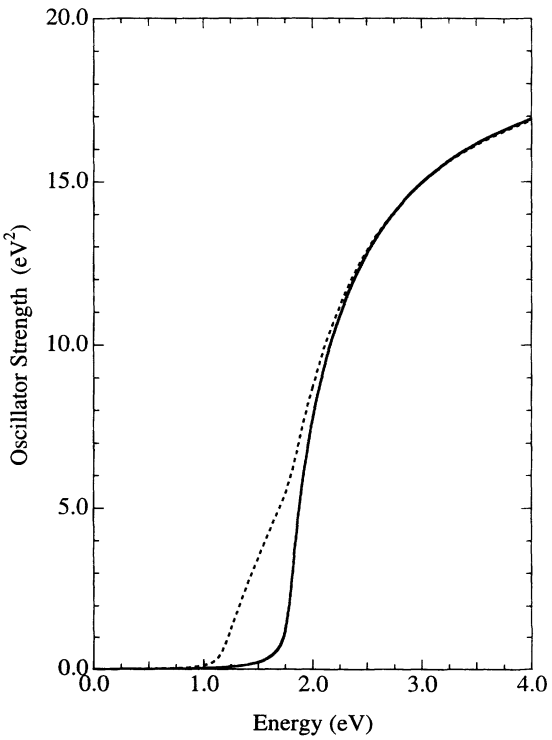

FIG. 9. The total integrated oscillator strength, which for both the rigid lattice and the infinite chain with nonlinear zero-point motion, asymptotically approaches $\frac{1}{8}W^2$, where $W = 2\Delta_0(\xi_0/a)$ is the $\pi - \pi^*$ bandwidth (Ref. 42).

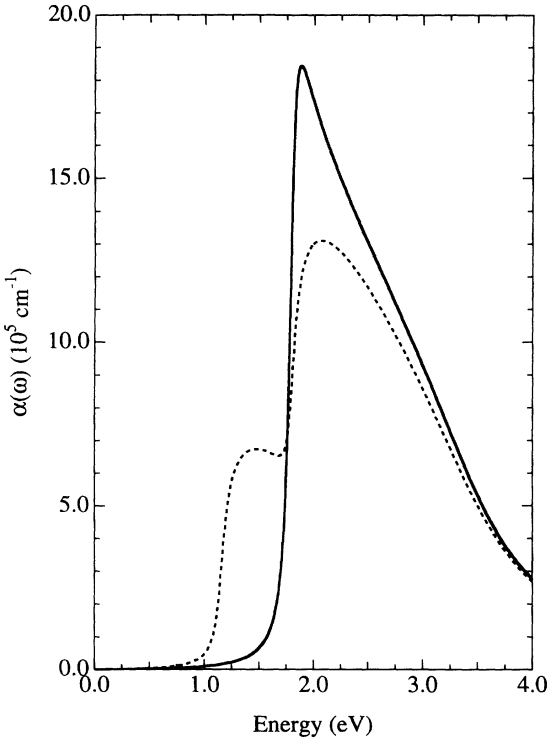

FIG. 10. The absorption coefficient calculated from the linear susceptibility for both the rigid-lattice (bold) and the lattice with nonlinear zero-point motion (dotted). The detailed shape of the shoulder on the leading edge of the degenerate-ground-state spectrum is a strong function of the quantum lattice fluctuation amplitude (see Sec. VIII B).

the first energy derivative of the unperturbed absorption line shape, is strongly anisotropic, and enhanced and redshifted relative to the nonoriented material, presumably due to an increase in structural order. The data support the notion that the low-energy feature, which is seen only in the degenerate-ground-state isomer, is intrinsic to the one-dimensional π-electron system.

Although, by comparison, the shoulder appears somewhat exaggerated in the theoretical curve, we emphasize that the detailed shape is found to be quite sensitive to both the quantum lattice fluctuation amplitude and the functional form of the ground state lattice wave function $\phi_0(s)$. By making small corrections to the ground state lattice wave function, curves can be generated which more closely resemble experimental data. These modifications to the absorption line shape are described below in Sec. VIII B and are plotted in Fig. 15.

The general agreement between the contribution to $\alpha(\omega)$ from direct photoproduction of charged soliton pairs with the experimental results for *trans*-$(CH)_x$ provides a quantitative measure of the accuracy with which we have treated the nonlinear Franck-Condon problem. Although approximate, the treatment of the ground state and the quantum lattice fluctuations is sufficiently accurate to reproduce the essential features and scale of the linear optical data.

VII. SSH THIRD-ORDER NONLINEAR SUSCEPTIBILITY

A. Rigid-lattice contribution

Since it is our purpose to demonstrate the enhancement to the nonlinear optical response by considering $S\bar{S}$ intermediate states, we begin by evaluating the expression for the generalized third-order nonlinear susceptibility $\chi^{(3)}(\omega_\sigma)$ of the rigid lattice in the absence of zero-point motion by considering the following sequences of virtual transitions (see Sec. II and Appendix F):

$$\langle G|\mathbf{y}|K_I\rangle\langle K_I|\mathbf{y}|K_{II}\rangle\langle K_{II}|\mathbf{y}|K_I\rangle\langle K_I|\mathbf{y}|G\rangle, \tag{34}$$

$$\langle G|\mathbf{y}|K_I\rangle\langle K_I|\mathbf{y}|G\rangle\langle G|\mathbf{y}|K_I\rangle\langle K_I|\mathbf{y}|G\rangle. \tag{35}$$

By adding the two contributions and substituting in terms of the dimensionless variables defined above, the expression for the rigid-lattice contribution to the third-order nonlinear optical susceptibility $\chi^{(3)}(\omega_\sigma)$ becomes

$$\chi^{(3)}_{\mathrm{RL}}(z_\sigma) = |\chi^3_0|_{\mathrm{RL}} \int dZ \, \frac{1}{|x|^8} \frac{1}{(x-z_\sigma)(x-z_1)} \times \left[\frac{1}{(2x-z_1-z_2)} - \frac{1}{(x-z_3)}\right], \tag{36}$$

with the rigid-lattice third-order prefactor given by

$$|\chi^3_0|_{\mathrm{RL}} = 4\,\frac{1}{\pi}\,e^4\,(f^0_{cv})^4\,\sigma\,\left(\frac{1}{2\Delta_0}\right)^2\,\rho^0_{cv} = 2.7 \times 10^{-10}\ \text{esu}. \tag{37}$$

The factor of 4 appearing in Eq. (37) is due to the spin degeneracy and is contained within the definition of the wave functions. The magnitude of the rigid-lattice prefactor scales like Δ_0^{-6}, and, using $2\Delta_0 = 1.8$ eV, compares favorably to that calculated by Agrawal *et al.*, who reported 3.2×10^{-10} esu.[9]

For the specific case of third-harmonic generation, Eq. (36) reduces to

$$\chi^{(3)}_{\mathrm{RL}}(3z) = -\frac{1}{2}|\chi^3_0|_{\mathrm{RL}} \int dZ \, \frac{1}{|x|^8} \frac{1}{(x-3z)(x-z)(x-z)}. \tag{38}$$

The minus sign appearing in Eq. (38) is in direct contradiction with the measured electroabsorption spectra,[21,22] which, for both *cis*- and *trans*-polyacetylene, demonstrate conclusively that the real and imaginary components of $\chi^{(3)}(\omega;\omega,\Omega,\Omega)$ are positive below the first resonance.[64] From the structural form of the generalized third-order nonlinear susceptibility, Eq. (2) in Sec. II, it is apparent that the same preresonant behavior must hold for any third-order nonlinear process.

B. A_g symmetric $S\bar{S}$ intermediate state contribution

The process considered involves the A_g symmetric $S\bar{S}$ electron-lattice configurations as an intermediate state in the perturbation theory expansion:

$$\langle G|\mathbf{y}|K_I\rangle\langle K_I|\mathbf{y}|S\bar{S}^0\rangle\langle S\bar{S}^0|\mathbf{y}|Q_I\rangle\langle Q_I|\mathbf{y}|G\rangle. \quad (39)$$

The independent sum over k and q is a consequence of the localized nature of the gap-state wave functions, which, in third order, allows scattering from one Bloch state $|K_I\rangle$ to another $|Q_I\rangle$. Using the results of Appendix G, the dominant term in the expression for $\chi^{(3)}(\omega_\sigma)$ can be written as follows:

$$\chi^{(3)}_{S\bar{S}}(\omega_\sigma) = e^4 \frac{1}{V}\sum_k\sum_s\sum_q N_s(s) \frac{\langle G|\mathbf{y}|K_I\rangle\langle K_I|\mathbf{y}|S\bar{S}^0\rangle\langle S\bar{S}^0|\mathbf{y}|Q_I\rangle\langle Q_I|\mathbf{y}|G\rangle}{[E_{cv}(k)-\omega_\sigma][E^2_{s\bar{s}}(s)-\omega_1-\omega_2][E_{cv}(q)-\omega_1]}. \quad (40)$$

Again, the factor $N_s(s)$ is a result of the lattice being able to statistically support $N_s(s)$ energetically degenerate $S\bar{S}$ intermediate state configurations for a given separation s. Converting the sums to integrals yields

$$\chi^{(3)}_{S\bar{S}}(z_\sigma) = |\chi^{(3)}_0|_{S\bar{S}} \int ds\, \bar{K}_0 \frac{|\phi_0(s)|^2}{(w_2 - z_1 - z_2)} \times \int dZ \frac{1}{|x|^3}\frac{G(s,x)}{(x - z_\sigma)} \times \int dZ' \frac{1}{|x'|^3}\frac{G(s,x')}{(x' - z_1)}, \quad (41)$$

where $x' = E_{cv}(q)/2\Delta_0$ and $Z' = Z(x')$. The prefactor of the neutral $S\bar{S}$ contribution to $\chi^{(3)}(\omega_\sigma)$ is given by

$$|\chi^{(3)}_0|_{S\bar{S}} = \rho^0_s \times 4\, e^4 \frac{1}{\pi^2}(f^0_{cv})^4\, \sigma\left(\frac{1}{2\Delta_0}\right) a\, I^4_0\, (\rho^0_{cv})^2 = \rho^0_s \times 1.5\times 10^{-8}\ \text{esu}. \quad (42)$$

For the specific case of third-harmonic generation Eq. (41) reduces to

$$\chi^{(3)}_{S\bar{S}}(3z) = |\chi^{(3)}_0|_{S\bar{S}} \int ds\, \bar{K}_0 \frac{|\phi_0(s)|^2}{(w_2 - 2z)} \times \int dZ \frac{1}{|x|^3}\frac{G(s,x)}{(x - 3z)} \times \int dZ' \frac{1}{|x'|^3}\frac{G(s,x')}{(x' - z)}. \quad (43)$$

Computational approximation

In order to avoid a possibly nonphysical divergence in the evaluation of Eqs. (41) and (43), we have omitted the $(w_2^* - x)$ term in the denominator of the dipole moment matrix element between the free electron-hole pair states and the A_g symmetric $S\bar{S}$ electron-lattice intermediate state [see Eq. (G3)]. For a well-separated $S\bar{S}$ pair, where $2\Delta_0 w_2 \approx 4\Delta_0/\pi$, this approximation underestimates the oscillator strength enhancement associated with the $S\bar{S}$ intermediate state contribution to $\chi^{(3)}(\omega_\sigma)$ by a factor of roughly π^2.

C. The relaxation of the vertical interband selection rule

In the calculation of the linear and third-order nonlinear susceptibilities presented in Secs. VI and VII we assumed a strict vertical wave vector selection rule for the interband dipole moment matrix elements. Due to the momentum of the photon this selection rule is somewhat relaxed in the infinite chain; i.e., the momentum of the photon becomes significant only when the conjugation length is on the order of the wavelength of the applied field. In Appendix F we show that the relaxation of the vertical selection rule effectively doubles the interband transition strength for each independent complete set of states that we sum over. Hence we need to multiply the linear and nonlinear susceptibility prefactors, Eqs. (23) and (29) and Eq. (37) and (42), by a factor of 2^p, where p is the number of independent momentum degrees of freedom for a given linear or nonlinear process. In the linear susceptibility calculation both the rigid-lattice and the $S\bar{S}$ contributions have one momentum degree of freedom. Hence the relaxation of the interband selection

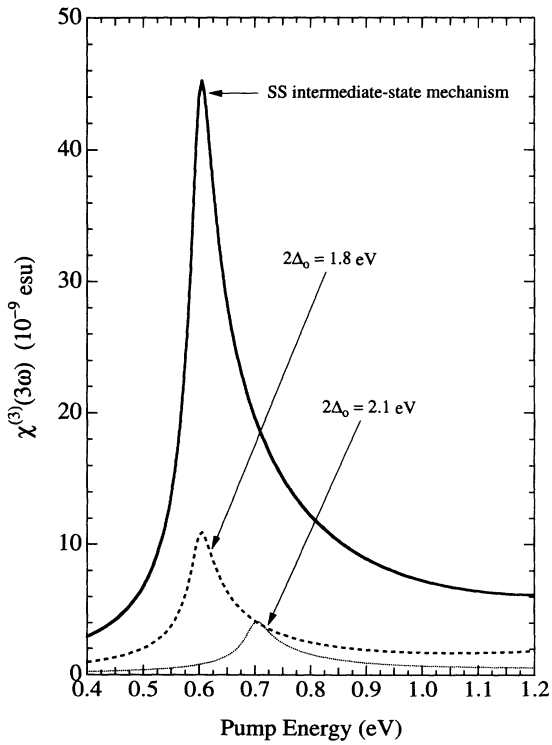

FIG. 11. The rigid-lattice and $S\bar{S}$ contributions to $\chi^{(3)}(3\omega)$. The rigid-lattice contribution was evaluated for both $2\Delta_0 = 2.1$ eV and $2\Delta_0 = 1.8$ eV, corresponding to *cis*- and *trans*-polyacetylene, respectively. The magnitude of the $S\bar{S}$ contribution is additionally enhanced due to a double resonance at 0.6 eV, where $3\omega = 2\Delta_0$ and $2\omega = 4\Delta_0/\pi$.

rule leaves the linear susceptibility prefactor ratio unchanged and, therefore, the oscillator strength remains conserved. In the calculation of $\chi^{(3)}(\omega_\sigma)$ the rigid-lattice contribution has two degrees of momentum freedom (one for each electron-hole pair), while the $S\bar{S}$ contribution has three (two electron-hole pairs and the localized $S\bar{S}$ wave function). The nonlinear susceptibility prefactor ratio becomes

$$\frac{|\chi_0^{(3)}|_{S\bar{S}}}{|\chi_0^{(3)}|_{\mathrm{RL}}} = \rho_s^0 \pi \, I_0^2, \tag{44}$$

which is twice as large as the ratio found for the linear susceptibility prefactors. For the maximum effective density of soliton-antisoliton pairs in the ground state, $\rho_s^0 = \rho_s^{\max}$, the nonlinear susceptibility prefactor ratio, Eq. (44), is equal to $4\Delta_0/(4\Delta_0/\pi) = \pi$, demonstrating that the enhancement to the nonlinear susceptibility from the $S\bar{S}$ intermediate state mechanism, as shown in Fig. 11, is a result of a true redistribution of oscillator strength rather than an anomalously large numerical prefactor.

VIII. RESULTS AND DISCUSSION

Figure 11 shows the results of a numerical integration of Eq. (43), the $S\bar{S}$ intermediate state contribution, and Eq. (38), the rigid-lattice contribution to $\chi^{(3)}(3\omega)$. The parameters used in the calculation of the nonlinear susceptibility are identical to those used in the linear susceptibility calculation. A second curve generated for the rigid-lattice model was evaluated assuming $2\Delta_0 = 2.1$ eV and $\xi_0 = W/2\Delta_0$; parameters appropriate for *cis*-$(CH)_x$. In all of the calculated spectra, we have assumed a common lifetime broadening parameter for all of the excited states: $\Gamma_k = \Gamma_s^0 = \Gamma_s^{\pm} = 0.10$ eV, corresponding to an excited state lifetime of roughly 10 fs. This value is consistent with both the Su-Schrieffer mechanism[27] and the decay of the high energy peak observed in the transient photoinduced absorption spectroscopy of Shank *et al.*[65]

The results demonstrate that the inclusion of nonlinear zero-point motion yields a significant enhancement of $\chi^{(3)}(3\omega)$ in systems with a degenerate ground state. From the preceding discussion, it is clear that this enhancement in the nonlinear susceptibility is a direct result of oscillator strength conservation; the nonlinear zero-point motion facilitates a transfer of oscillator strength from states with energies above the band gap to states with energies below the band gap, and virtual transitions involving these lower energy states result in a corresponding larger hyperpolarizability. Note that the $S\bar{S}$ intermediate state contribution is positive and larger than the rigid-lattice contribution at all frequencies, thus reversing the overall sign and making both the real and imaginary components of $\chi^{(3)}(\omega_\sigma)$ positive below the first resonance.

A. Electron-electron interactions

The proper description of the $S\bar{S}$ intermediate state requires taking into account both electron-electron interactions and electron-phonon interactions. The effects of electron-electron interactions on the ordering of the energy eigenstates is well known for polyene oligomers, tending to lower the energy of the $2A_g$ state relative to that of the $1B_u$ state.[66] To simulate the possible effects of electron-electron interactions on the $S\bar{S}$ contribution to $\chi^{(3)}(3\omega)$, we assume in our numerical calculations that

$$E_{S\bar{S}}^2 \Rightarrow E_{S\bar{S}}^2 - 2\Delta_0 \, \alpha \, |O(s)|^2, \tag{45}$$

where α defines the magnitude of the Coulomb interaction and $O(s)$ is the overlap of the gap-state wave functions centered on S and $\bar{S}$, respectively,

$$O(s) = \frac{K_0}{2} \int dy \, \mathrm{sech}[K_0(y + R/2)] \, \mathrm{sech}[K_0(y - R/2)] = \frac{s}{\sinh(s)}. \tag{46}$$

Thus $E_{S\bar{S}}^2(s) = (2 - \alpha)E_g$ for $s = 0$ and approaches $E_{S\bar{S}}^2(s) = (2/\pi)E_g$ as $s \Rightarrow \infty$. Equation (45) is clearly an assumption; it is, however, qualitatively correct in the two limits; for $s \Rightarrow 0$, correlation effects reduce the energy of the A_g excited state to be intermediate between $2\Delta_0$ and $4\Delta_0$,[67] and for $s \Rightarrow \infty$, the neutral pair will only be affected by long range Coulomb interactions which should be well screened in the solid state. The potential energy surface of the neutral $S\bar{S}$ configuration for $\alpha = 0.00$, $\alpha = 0.50$, and $\alpha = 0.85$ are shown as the dotted, dashed, and solid lines, respectively, in Fig. 12.

Numerical integration of Eq. (43) for various values of the correlation parameter α have been carried out.

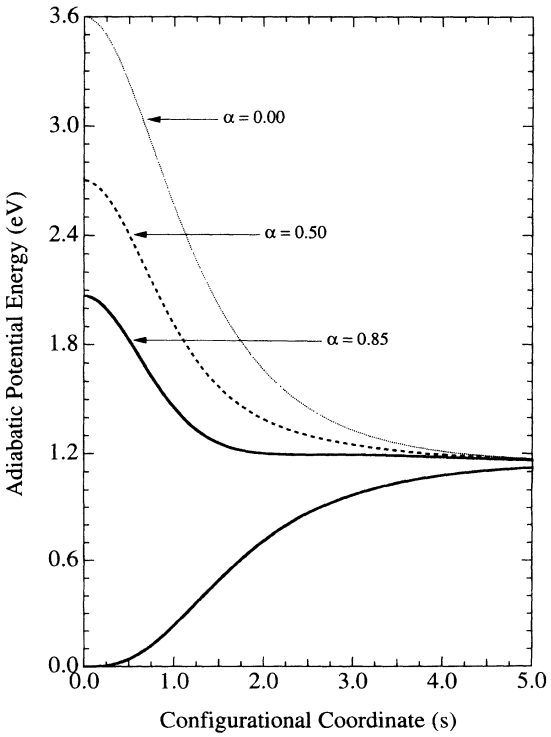

FIG. 12. The effects of the phenomenological electron-electron interaction [Eq. (45)] on the configurational potential surfaces of a degenerate-ground-state polymer.

The dotted curve in Fig. 13 is a plot of the $S\bar{S}$ intermediate state contribution without electron correlation (i.e., $\alpha = 0$), the dashed curve corresponds to $\alpha = 0.50$, and the heavy solid curve in Fig. 13 corresponds to $\alpha = 0.85$. Figure 13 demonstrates the additional enhancement gained by reducing $E^2_{S\bar{S}}(s)$ for small s, so that the double resonance condition is satisfied over a wider range of the configurational coordinate.

B. Quantum lattice fluctuation amplitude

To examine the effects of the quantum lattice fluctuation amplitude on the linear and nonlinear optical susceptibility, the ground state lattice wave function is modified as follows:

$$|\phi_0(s)|^2 = \frac{1}{\sqrt{2\pi}} \exp\left[-\frac{1}{2}\, s^2\right] \Rightarrow \frac{1}{\sqrt{2\pi}\sigma_s} \exp\left[-\frac{1}{2}\,(s/\sigma_s)^2\right]. \quad (47)$$

The inset in Fig. 14 shows the percent reduction in the classical dimerization as a function of the quantum lattice fluctuation amplitude σ_s while assuming the maximum density of $S\bar{S}$ pairs that the system can support; $\rho^0_s = \rho^{\max}_s$. The results of the various Monte Carlo simulations[56–59] fall between the two horizontal lines and a fully dense neutral soliton lattice yields a reduction in the classical dimerization of roughly 56%. The inset demonstrates that our initial model of the $S\bar{S}$ probability distribution, Eq. (17), is at the upper limit of the Monte Carlo results.

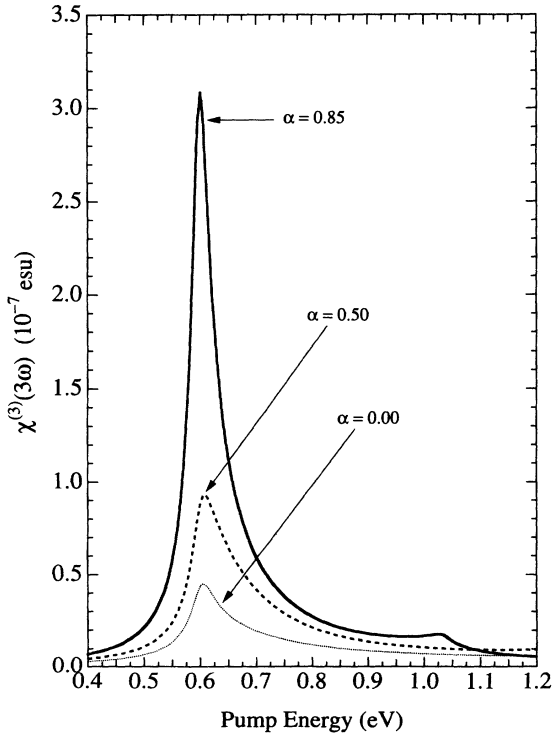

FIG. 13. The $S\bar{S}$ intermediate state mechanism contribution to $\chi^{(3)}(3\omega)$ resulting from the configurational potential energy surfaces shown in Fig. 12. The results demonstrate the sensitivity of $\chi^{(3)}$ to the details of the potential energy surface of the A_g symmetric neutral $S\bar{S}$ pair.

In Fig. 14 we plot the magnitude of $\chi^{(3)}(3\omega)$ evaluated at 0.6 eV as a function of the percent reduction in the dimerization amplitude $-\delta u/u_0$. Over the 5–20 % range, the curve shows a linear relationship between the magnitude of the nonlinear susceptibility and the reduction in the dimerization amplitude, and $\chi^{(3)}(3\omega)$ is found to vary by less than a factor of 2.

The effects of the quantum lattice fluctuation amplitude on the linear optical absorption coefficient are shown in Fig. 15 for several values of σ_s, corresponding to a 5–20 % reduction in the dimerization amplitude. Note that with $-\delta u/u_0 = 15\%$, the absorption line shape more closely resembles that measured experimentally. Figures 14 and 15 demonstrate that the absorption edge can be significantly modified without quenching the $S\bar{S}$ intermediate state mechanism.

C. Confinement

In systems which do not have a degenerate ground state (e.g., *cis*-polyacetylene) the configurational poten-

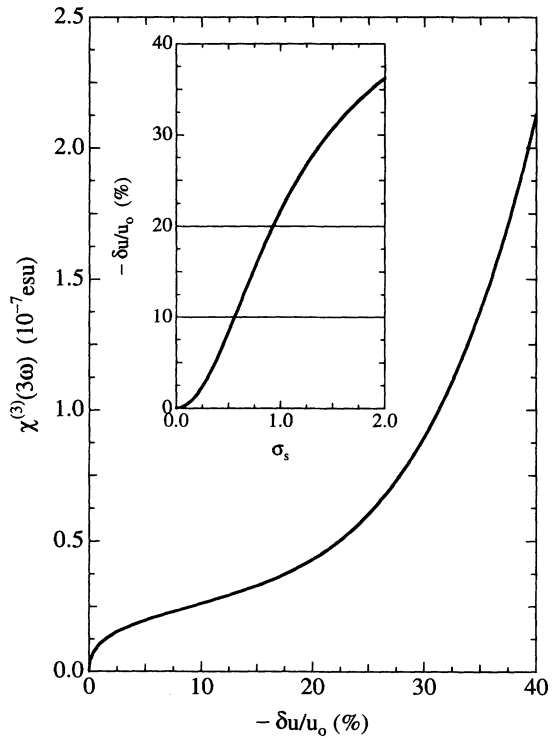

FIG. 14. Inset: the percent reduction in the classical dimerization $-\delta u/u_0$ as a function of the nonlinear zero-point amplitude σ_s. The range spanned by the various Monte Carlo simulations (Refs. 56–59) is defined by the two horizontal lines, and a symmetric neutral soliton lattice yields a reduction of roughly 56%. Main figure: the magnitude of $\chi^{(3)}(3\omega)$ evaluated at 0.6 eV as a function of the reduction in the classical dimerization amplitude. Note that $\chi^{(3)}(3\omega)$ varies by less than a factor of 2 over the 5–20 % range. Both curves assume the maximum density of $S\bar{S}$ pairs $\rho^0_s = \rho^{\max}_s$ [see Eqs. (19) and (47)].

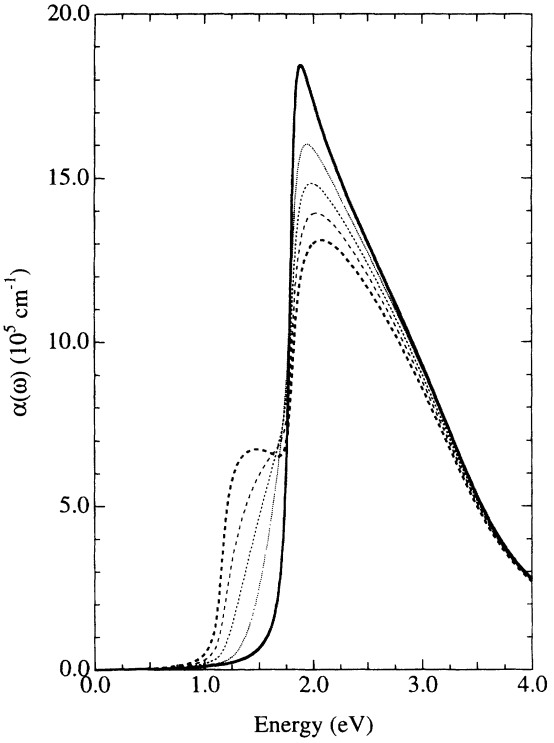

FIG. 15. The absorption coefficient for the degenerate ground state calculated from Eq. (33) using several values for the nonlinear zero-point amplitude, corresponding to a 5%, 10%, 15%, and 20% reduction in the classical dimerization amplitude, respectively. Over this same range, the magnitude of $\chi^{(3)}(3\omega)$ changes by less than a factor of 2. The absorption coefficient calculated for the rigid lattice is also shown for comparison.

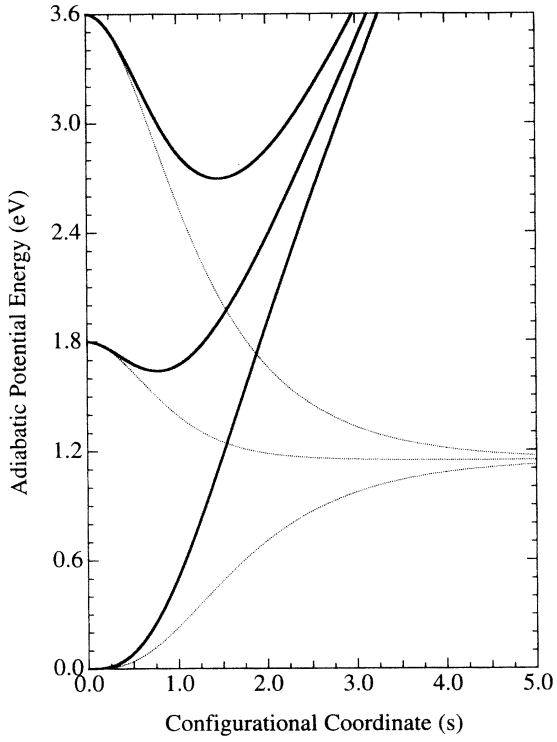

FIG. 16. The configurational potential energy surfaces for a nondegenerate ground state (bold) and a degenerate ground state (dotted). The linear confinement potential of the nondegenerate ground state leads to the appearance of excited states with a locally stable lattice configuration; A_g and B_u symmetric polaron excitons. A significant Stokes shift in the photoluminescence excitation spectrum would indicate that the ground-state lattice wave function does not strongly overlap that of the relaxed B_u symmetric polaron exciton (Ref. 23).

tial energy, Eq. (11), must be augmented by the confinement potential[36,37]

$$E^{\nu}_{S\bar{S}} \Rightarrow E^{\nu}_{S\bar{S}} + \gamma\frac{4\Delta_0}{\pi}[s - \tanh(s)], \tag{48}$$

where γ, the confinement parameter, is a measure of the amount by which the one-electron crystal potential lifts the ground state degeneracy. In Fig. 16, we plot the configurational potential energy surfaces for a nondegenerate-ground-state polymer generated from Eqs. (11) and (48) with $\gamma = 1$. For comparison, the corresponding curves for the degenerate ground state are also shown (dotted). The linear confinement potential quenches the amplitude of the nonlinear zero-point motion and leads to the appearance of bound excited states, A_g and B_u symmetric polaron excitons, which are described as confined soliton-antisoliton pairs. Note that "confinement" refers to the separation of the mass centers of the two kinks and does not imply a localization of the electronic wave function. In fact, the trend is just the opposite: as γ increases the localization length $L_{S\bar{S}}$ increases, and in the limit of infinite confinement, where $s \Rightarrow 0$, the $S\bar{S}$ wave function extends over the entire lattice and merges with the Bloch continuum at $\pm\Delta_0$ (see Sec. III B and Fig. 3).

The nondegenerate ground state quenches the $S\bar{S}$ intermediate state mechanism in the following ways.

(i) The linear confining potential quenches the amplitude of the nonlinear zero-point motion. A Franck-Condon analysis of the absorption, electroabsorption, and photoluminescence line shapes demonstrates that the potential energy surfaces of many nondegenerate-ground-state polymers, including *cis*-polyacetylene, are approximately harmonic and that the excited state relaxation is very weak.[18,23]

(ii) In the nondegenerate ground state polymer, the spectral density of the "confined" $S\bar{S}$ electronic wave function is strongly peaked at the band edge, $\pm\Delta_0$. Therefore, the amount of oscillator strength transferred from the vis-ultraviolet to the near-infrared for a given $S\bar{S}$ pair is substantially reduced.

(iii) Phase space filling in nondegenerate-ground-state systems: since the minimum coherence length of the $S\bar{S}$ wave function (polaron-exciton) in the nondegenerate-ground-state polymer is larger than that of the well-separated $S\bar{S}$ pair in the degenerate-ground-state polymer, the effective density of $S\bar{S}$ pairs in the ground state is substantially reduced. Equation (9) states that in the limit of infinite confinement the volume of the $S\bar{S}$ phase

space approaches zero.

(iv) Since the energy of the A_g symmetry state in the nondegenerate-ground-state polymer is lifted by the one-electron crystal potential (see Fig. 16) the oscillator strength enhancement to the nonlinear susceptibility is diminished.

(v) The third-harmonic nonlinear response in the nondegenerate-ground-state polymer is further reduced by a lifting of the simultaneous two- and three-photon resonance by the one-electron crystal potential.

Using the results of Secs. VI and VII, one can show that a simple ratio exists between the magnitudes of the linear and third-order nonlinear optical susceptibilities in the NRL model

$$\left.\frac{\chi^{(3)}_{\mathrm{RL}}(3\omega)}{\chi^{(1)}_{\mathrm{RL}}(\omega)}\right|_{\omega=2\Delta_0} \sim \left(\frac{e}{2\Delta_0} f^0_{cv}\right)^2 \approx 10^{-10}\ \text{esu}. \qquad (49)$$

The data presented by Halvorson *et al.*[2] show that for *cis*-$(CH)_x$, this ratio is of the right order of magnitude, suggesting that *cis*-$(CH)_x$ is accurately described by the rigid-lattice model. This is consistent with our expectations, since the nondegenerate ground state of the *cis* isomer must suppress the nonlinear component of the lattice zero-point motion which enables the $S\bar{S}$ intermediate state mechanism. The relatively sharp photoluminescence excitation threshold and 0.15 eV Stokes shift reported in Ref. 16 demonstrate that the ground state lattice wave function does not overlap the relaxed configuration of the luminescent polaron exciton; if the nonlinear Franck-Condon factor was of any significance, relaxed configuration of the polaron exciton could be excited directly and a subgap excitonic feature would be visible in the linear absorption spectrum.[33] For *pure cis*-$(CH)_x$, there is no evidence of significant subgap optical absorption and certainly no evidence of a sharp absorption resonance at the photoluminescence energy. We therefore conclude that in *cis*-$(CH)_x$ the nonlinear component of the lattice zero-point motion is quenched by the nondegenerate ground state.

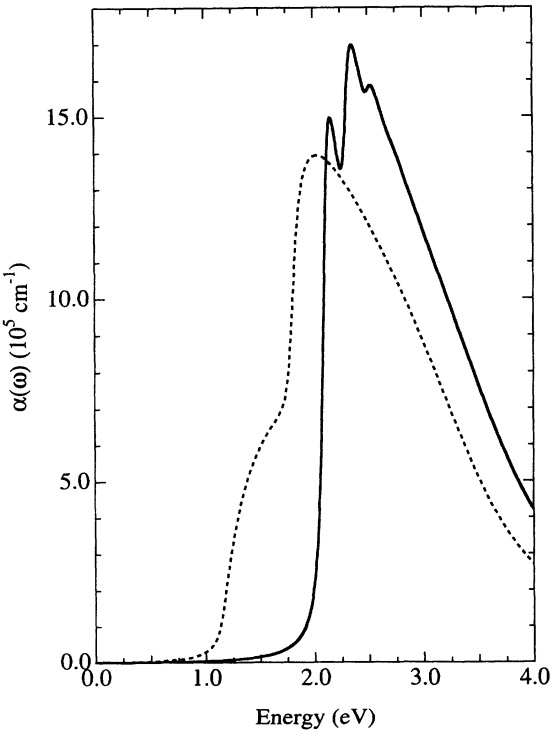

FIG. 17. The absorption coefficient calculated for a nondegenerate-ground-state conjugated polymer (bold line) demonstrating the typically observed "displaced-harmonic-oscillator" vibronic progression. For comparison, the absorption coefficient calculated for the degenerate-ground-state conjugated polymer with $-\delta u/u_0 = 15\%$ (dotted line) is also shown.

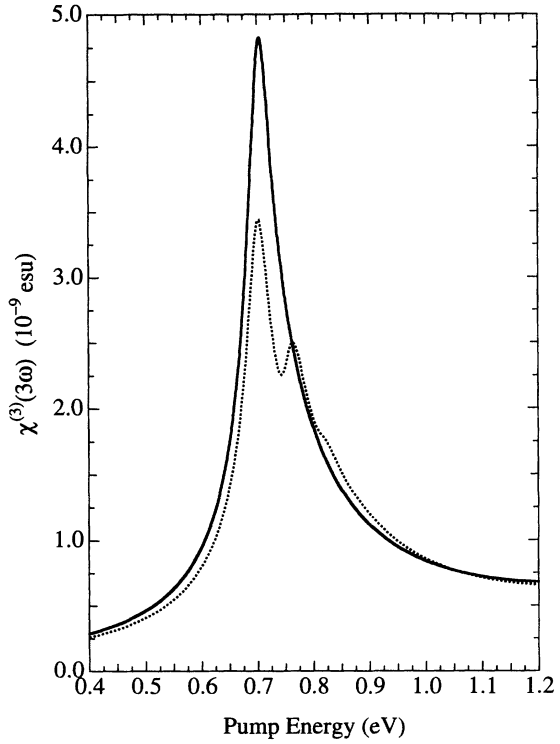

FIG. 18. The nonlinear susceptibility $\chi^{(3)}(3\omega)$ calculated for the rigid lattice (bold line) and in the harmonic approximation assuming $\hbar\omega_{ph} = 0.19$ eV and $S = 0.4$ (dashed line).

We emphasize that the *harmonic* component of the lattice zero-point motion is observable in the optical spectra of the nondegenerate-ground-state polymer. The degeneracy lifting effects of the confinement potential result in a relatively harmonic configurational potential energy surface, e.g., a dominant intra-unit-cell optical mode, which is characterized by the simple "displaced-harmonic-oscillator" vibronic progressions observed in the absorption, electroabsorption, and photoluminescence spectra of nondegenerate-ground-state polymers and oligomers.[16,18,19,21–23,68] In Fig. 17, we show the effects of *harmonic* quantum lattice fluctuations on the optical absorption line shape using parameters appropriate for *cis*-$(CH)_x$; we use a phonon energy of 0.19 eV and a Huang-Rhys parameter of $S = 0.4$. There is excellent agreement between the positioning of the vibronic features and the overall shape of the calculated absorption line shape and that measured experimentally.[16,18,19,21,22]

The effects of this vibronic coupling are also observed in the third-order optical response. Vibronic features are readily observed in the electric field modulation spectra $\chi^{(3)}(\omega,0,0)$, of both *cis*- and *trans*-polyacetylene.[22] Figure 18 demonstrates the effects of vibronic coupling on the THG line shape; however, to actually observe these features would require a much larger signal to noise ratio than is currently avaliable in THG spectroscopy.

IX. CONCLUSION

We have presented a calculation of the linear and third-order nonlinear optical susceptibility based on a symmetry specific mechanism which focuses on the differences between degenerate- and nondegenerate-ground-state conjugated polymers. In doing this, we have developed an approximate formulation for describing the quantum lattice fluctuations in the degenerate ground state in terms of a single collective configurational coordinate $s \equiv K_0 R$, representing simultaneously the separation, coherence length, and number density of virtual soliton-antisoliton electron-lattice configurations on the polymer chain.

Using this approximate description of the ground state, we have calculated both the linear and the third-order nonlinear optical susceptibility $\chi^{(1)}(\omega)$ and $\chi^{(3)}(\omega_\sigma)$, for the rigid lattice and the infinite chain with nonlinear zero-point motion. Our results demonstrate that for systems with a degenerate ground state, contributions from $S\bar{S}$ intermediate states enabled by nonlinear zero-point motion make important contributions to both the linear and the third-order nonlinear optical response.

(i) With the inclusion of nonlinear zero-point motion, a feature appears on the low-energy side of the linear susceptibility spectrum corresponding to the direct photoproduction of charged soliton-antisoliton pairs. The oscillator strength associated with the direct photoproduction of charged solitons pairs comes at the expense of that associated with interband transition; total oscillator strength is conserved.

(ii) For any third-order process, contributions arising from A_g symmetric neutral $S\bar{S}$ pair configurations as intermediate states are one to two orders of magnitude larger than the corresponding rigid-lattice contribution. The large contribution to $\chi^{(3)}(\omega_\sigma)$ from the $S\bar{S}$ intermediate states results from the large transition dipole moment between the free electron-hole pair excited states of B_u symmetry and the A_g symmetric neutral $S\bar{S}$ excited state. This enhanced transition dipole moment is a consequence of the large virtual shifts of oscillator strength associated with the localized $S\bar{S}$ electron-lattice configuration. For third-harmonic generation, $\chi^{(3)}(3\omega)$ is further enhanced by a condition unique to degenerate-ground-state systems, simultaneous two- and three-photon resonance (see Fig. 11 caption).

These contributions to $\chi^{(1)}(\omega)$ and $\chi^{(3)}(\omega_\sigma)$ are both enabled by nonlinear zero-point motion which provides a finite Franck-Condon overlap between the ground and $S\bar{S}$ excited state lattice wave functions. Since confinement quenches the nonlinear zero-point motion, the $S\bar{S}$ intermediate state mechanism is specific to the symmetry of the ground state.

The general agreement of the calculated linear optical coefficients with those measured experimentally provides a quantitative measure of the accuracy with which we have treated the nonlinear Franck-Condon factor; the treatment of the ground state lattice zero-point motion and Franck-Condon overlap factor is sufficiently accurate to reproduce the essential features and scale of the linear optical data. Furthermore, the contribution to the third-order nonlinear optical susceptibility from the $S\bar{S}$ intermediate state mechanism is numerically consistent with the experimental values, i.e., $10^{-8}-10^{-7}$ esu, obtained from third-harmonic generation and electroabsorption studies of highly oriented and structurally ordered *trans*-polyacetylene.

We conclude that in degenerate-ground-state conjugated polymers nonlinear zero-point motion provides an effective mechanism to facilitate large (virtual) shifts of oscillator strength from the vis-ultraviolet to the near-infrared, which results in both subgap optical absorption and photoconductivity, as well as a significantly enhanced third-order nonlinear susceptibility. The *cis*/*trans* comparative THG and photoconductivity studies are consistent with the model presented here, in which both the linear and third-order nonlinear optical response of degenerate-ground-state conjugated polymers are dominated by $S\bar{S}$ electron-lattice configurations enabled by nonlinear zero-point motion.

ACKNOWLEDGMENTS

This research was supported by the National Science Foundation through Grant No. NSF DMR90-12808. We thank A. R. Bishop, N. Bulut, J. L. Bredas, D. K. Campbell, E. Ehrenfreund, C. Halvorson, D. Hone, S. Kivelson, S. Mazumdar, D. McBranch, R. H. Mc Kenzie, K. Pakbaz, Z. Shuai, M. Sinclair, W. P. Su, and G. Yu for important comments and discussions.

APPENDIX A: TLM WAVE FUNCTIONS

1. Extended band states

The TLM one-electron energy spectrum is given by[35,37]

$$\epsilon(k) = \pm\epsilon_k = \pm\Delta_0\sqrt{(k\xi_0)^2+1}. \tag{A1}$$

The two-component spinors defining the valence and conduction band continuum are defined by[37]

$$\psi_k^v = \begin{pmatrix} U_k^v \\ V_k^v \end{pmatrix}, \qquad \psi_k^c = \begin{pmatrix} U_k^c \\ V_k^c \end{pmatrix}, \tag{A2}$$

where

$$U_k^v = -N_D(k)(1-A)e^{iky}, \quad V_k^v = -N_D(k)(1+A)e^{iky},$$
$$U_k^c = -iN_D(k)(1+A)e^{iky}, \quad V_k^c = +iN_D(k)(1-A)e^{iky}, \tag{A3}$$

and

$$N_D(k)=\frac{1}{2\sqrt{L}}\left[\frac{\epsilon_k-\Delta_0}{\epsilon_k}\right]^{1/2},$$
$$A=\frac{k\xi_0\Delta_0}{\epsilon_k-\Delta_0}. \tag{A4}$$

2. $S\bar{S}$ midgap levels

The localized spinor wave functions associated with a $S\bar{S}$ pair of arbitrary separation $R=2y_0$ and center of mass coordinate Y are given by[37]

$$\begin{aligned}U_{-\omega_0}&=\tfrac{1}{2}N_p^0[(1+i)S_- -(1-i)S_+],\\ V_{-\omega_0}&=\tfrac{1}{2}N_p^0[(1-i)S_- -(1+i)S_+],\\ U_{\omega_0}&=\tfrac{1}{2}N_p^0[(1+i)S_- +(1-i)S_+],\\ V_{\omega_0}&=\frac{1}{2}N_p^0[(1-i)S_- +(1+i)S_+],\end{aligned} \tag{A5}$$

where

$$S_\pm=\mathrm{sech}[K_0(y\pm y_0-Y)] \tag{A6}$$

and

$$N_p^0=\frac{1}{2}\sqrt{K_0}. \tag{A7}$$

APPENDIX B: TLM BASIS TRANSFORMATION

1. Basic overlap integrals

In evaluating the overlap integrals necessary for the basis transformation used in calculating the $S\bar{S}$ contribution to the linear and nonlinear optical susceptibility, the following integral is encountered:

$$\begin{aligned}F_\pm&=\int dy\; e^{iky}\;\mathrm{sech}[K_0(y\pm y_0-Y)]\\ &=\frac{\pi}{K_0}\mathrm{sech}\left(\frac{\pi}{2}\frac{k}{K_0}\right)\;e^{\mp iky_0}e^{ikY}\end{aligned} \tag{B1}$$

The overlap integrals projecting the single-particle midgap states onto the non-phase-shifted basis are defined as

$$\begin{aligned}\langle\psi_{\omega_0}(y)|\psi_k^c(y)\rangle&=I_1(k)\;e^{ikY},\\ \langle\psi_{\omega_0}(y)|\psi_k^v(y)\rangle&=I_2(k)\;e^{ikY},\\ \langle\psi_{-\omega_0}(y)|\psi_k^c(y)\rangle&=I_3(k)\;e^{ikY},\\ \langle\psi_{-\omega_0}(y)|\psi_k^v(y)\rangle&=I_4(k)\;e^{ikY},\end{aligned} \tag{B2}$$

with

$$\begin{aligned}I_1=I_4&=-i2N_p^0N_D(k)\frac{\pi}{K_0}\mathrm{sech}\left(\frac{\pi}{2}\frac{k}{K_0}\right)\\ &\quad\times[\sin(ky_0)+A\cos(ky_0)],\end{aligned} \tag{B3}$$

$$\begin{aligned}I_2=I_3&=-2N_p^0N_D(k)\frac{\pi}{K_0}\mathrm{sech}\left(\frac{\pi}{2}\frac{k}{K_0}\right)\\ &\quad\times[\cos(ky_0)-A\sin(ky_0)].\end{aligned}$$

The following definition is useful in demonstrating a wave vector selection rule for the dipole moment matrix element

$$I_2(k)I_2(q)+|I_1(k)I_1(q)|=\frac{1}{N}\;I_0^2\;G(s,k,q), \tag{B4}$$

where

$$I_0^2=\frac{1}{2}\left(\pi^2\frac{\xi_0}{a}\right). \tag{B5}$$

The diagonal component of Eq. (B4) is given by

$$\begin{aligned}\beta(s,k)&\equiv\frac{1}{N}\;I_0^2\;G(s,k,q)\delta_{k,-q}\\ &=\frac{1}{N}\;I_0^2\;\frac{1}{\bar{K}_0}\mathrm{sech}^2\left(\frac{\pi}{2}\frac{k\xi_0}{\bar{K}_0}\right).\end{aligned} \tag{B6}$$

2. Dimensionless overlap integrals

For computational purposes, it is convenient to recast the basis transformation defined in Eq. (B3) in terms of the dimensionless optical energy parameters $x=E_{cv}(k)/2\Delta_0$ and $Z=\sqrt{x^2-1}$. The overlap integrals become

$$\begin{aligned}I_1=I_4&=-i2N_p^0N_D(x)\frac{\pi}{K_0}\mathrm{sech}\left(\frac{\pi}{2}\frac{1}{\bar{K}_0}Z\right)\\ &\quad\times\left[\sin\left(\frac{R}{2\xi_0}Z\right)+A(x)\cos\left(\frac{R}{2\xi_0}Z\right)\right],\end{aligned} \tag{B7}$$

$$\begin{aligned}I_2=I_3&=-2N_p^0N_D(x)\frac{\pi}{K_0}\mathrm{sech}\left(\frac{\pi}{2}\frac{1}{\bar{K}_0}Z\right)\\ &\quad\times\left[\cos\left(\frac{R}{2\xi_0}Z\right)-A(x)\sin\left(\frac{R}{2\xi_0}Z\right)\right],\end{aligned}$$

where

$$N_D(x)=\frac{1}{2\sqrt{L}}\left[\frac{x-1}{x}\right]^{1/2},$$
$$A(x)=\frac{Z}{|x-1|}. \tag{B8}$$

It is useful to define the following diagonal component of Eq. (B4):

$$\beta(s,x)\equiv I_2^2(x)+|I_1(x)|^2=\frac{1}{N}\;I_0^2\;G(s,x), \tag{B9}$$

where

$$G(s,x)=\frac{1}{\bar{K}_0}\mathrm{sech}^2\left(\frac{\pi}{2}\frac{1}{\bar{K}_0}Z\right). \tag{B10}$$

APPENDIX C: MANY-BODY EIGENSTATES OF THE RIGID LATTICE

1. The ground state

$$|G\rangle=|g\rangle\otimes|\Phi_0\rangle. \tag{C1}$$

Because of the two-particle nature of the $S\bar{S}$ interme-

diate states, all matrix elements are calculated in the two-particle representation described below. One of the $N(N-1)$ two-particle momentum representation for the many-body ground state is found by factoring ψ_k^v and $\psi_{q\neq k}^v$ out of the ground state Slater determinant

$$|g\rangle = \sum_i \sum_{j\neq i} |\psi_k^v(y_i)\psi_{q\neq k}^v(y_j)\rangle \otimes |N-2\rangle \otimes \chi_0^s, \tag{C2}$$

where χ_0^s is the many-body singlet spin wave function henceforth suppressed and $|N-2\rangle$ is the vector spanning the valence band continuum not including ψ_k^v and $\psi_{q\neq k}^v$ subject to the normalization condition

$$\langle N-2|N-2\rangle = \frac{1}{N(N-1)}. \tag{C3}$$

2. The first excited state

$$|K_I\rangle = |k_I\rangle \otimes |\Phi_0\rangle. \tag{C4}$$

The first excited state is found by operating on the ground state with the operator $c_k^{c\dagger}c_k^v$

$$|k_I\rangle = c_k^{c\dagger}c_k^v|g\rangle. \tag{C5}$$

In the two-particle representation this becomes

$$|k_I\rangle = \frac{1}{\sqrt{2}} \sum_{i,j\neq i} [|\psi_k^c(y_i)\psi_{q\neq k}^v(y_j)\rangle + |\psi_{q\neq k}^v(y_i)\psi_k^c(y_j)\rangle] \times \otimes |N-2\rangle. \tag{C6}$$

3. The second excited state

$$|K_{II}\rangle = |k_{II}\rangle \otimes |\Phi_0\rangle. \tag{C7}$$

The second excited state is found by operating on the first excited state with the operator $c_q^{c\dagger}c_q^v$

$$c_q^{c\dagger}c_q^v c_k^{c\dagger}c_k^v|g\rangle. \tag{C8}$$

In the perturbation theory expansion for $\chi^{(3)}$, Soos *et al.* have shown that terms with $k \neq q$ correspond to disconnected diagrams and cancel exactly.[46] We therefore restrict our attention to the following spin-paired doubly excited states

$$|k_{II}\rangle = c_{k\sigma}^{c\dagger}c_{k\sigma}^v c_{k-\sigma}^{c\dagger}c_{k-\sigma}^v|g\rangle. \tag{C9}$$

The corresponding two-particle representation is given by

$$|k_{II}\rangle = \sum_{i,j\neq i} |\psi_{k\sigma}^c(y_i)\psi_{k-\sigma}^c(y_j)\rangle \otimes |N-2\rangle. \tag{C10}$$

APPENDIX D: MANY-BODY EIGENSTATES OF THE $S\bar{S}$ ELECTRON-LATTICE CONFIGURATION

1. The first excited B_u symmetric $S\bar{S}$ pair

The many-body wave function describing a single $S\bar{S}$ pair in the B_u symmetric electronic configuration is defined as the Born-Oppenheimer product

$$|S\bar{S}^{\pm}\rangle = |\Psi_{S\bar{S}}^{\pm}\rangle \otimes |\Phi_{\rm ex}(s,Y)\rangle. \tag{D1}$$

By taking the tensor product of the upper and lower gap state and the phase-shifted continuum, we find an expression for the B_u symmetric $S\bar{S}$ many-body electronic wave function in the two-particle representation

$$|\Psi_{S\bar{S}}^{\pm}(s)\rangle = \frac{1}{\sqrt{2}} \sum_{i,j\neq i} [|\psi_{\omega_0}(y_i)\psi_{-\omega_0}(y_j)\rangle + |\psi_{-\omega_0}(y_i)\psi_{\omega_0}(y_j)\rangle] \otimes |N-2_{\pm\omega_0}\rangle, \tag{D2}$$

where $|N-2_{\pm\omega_0}\rangle$ is the vector spanning the phase-shifted valence band: *2 is the number of electrons occupying the gap-state wave functions.* In the non-phase-shifted basis, Eq. (D2) becomes

$$|\Psi_{S\bar{S}}^{\pm}(s)\rangle = \frac{1}{\sqrt{2}} \sum_{i,j\neq i} \sum_{k,q\neq k} |N-2\rangle \otimes |\psi_{S\bar{S}}^{\pm}(s;y_i^k,y_j^q)\rangle \times e^{-i(k+q)Y}, \tag{D3}$$

where

$$\begin{aligned}|\psi_{S\bar{S}}^{\pm}(s;y_i^k,y_j^q)\rangle = &-[I_3(k)I_1(q) - I_1(k)I_3(q)]|\psi_k^v(y_i)\psi_q^v(y_j)\rangle + [I_3(k)I_2(q) - I_1(k)I_4(q)]|\psi_k^v(y_i)\psi_q^c(y_j)\rangle \\ &-[I_4(k)I_1(q) - I_2(k)I_3(q)]|\psi_k^c(y_i)\psi_q^v(y_j)\rangle + [I_4(k)I_2(q) - I_2(k)I_4(q)]|\psi_k^c(y_i)\psi_q^c(y_j)\rangle\end{aligned} \tag{D4}$$

and the vector $|N-2\rangle$ now spans the non-phase-shifted valence band continuum. Using the parity transformation properties of the valence and conduction band extended states,[37] one can show that $\Psi_{S\bar{S}}^{\pm}(s)$ is of B_u symmetry

$$\Pi\, \Psi_{S\bar{S}}^{\pm}(s)\, \Pi^{\dagger} = -\Psi_{S\bar{S}}^{\pm}(s). \tag{D5}$$

2. The second excited A_g symmetric $S\bar{S}$ pair

$$|S\bar{S}^0\rangle = |\Psi_{S\bar{S}}^0\rangle \otimes |\Phi_{\rm ex}(s,Y)\rangle. \tag{D6}$$

The many-body electronic wave function associated with the A_g symmetric $S\bar{S}$ configuration in the phase-shifted basis is given by

$$|\Psi^0_{S\bar{S}}(s)\rangle = \sum_{i,j\neq i} |\psi_{\omega_0}(y_i)\psi_{\omega_0}(y_j)\rangle \otimes |N-2_{\omega_0}\rangle. \quad \text{(D7)}$$

The corresponding many-body state in the non-phase-shifted basis is given by

$$|\Psi^0_{S\bar{S}}(s)\rangle = \sum_{i,j\neq i}\sum_{k,q\neq k} |N-2\rangle \otimes |\psi^0_{S\bar{S}}(s;y^k_i,y^q_j)\rangle \times e^{-i(k+q)Y}, \quad \text{(D8)}$$

where

$$\begin{aligned}|\psi^0_{S\bar{S}}(s;y^k_i,y^q_j)\rangle = &+I_3(k)I_3(q)|\psi^v_k(y_i)\psi^v_q(y_j)\rangle \\ &-I_3(k)I_4(q)|\psi^v_k(y_i)\psi^c_q(y_j)\rangle \\ &+I_4(k)I_3(q)|\psi^c_k(y_i)\psi^v_q(y_j)\rangle \\ &-I_4(k)I_4(q)|\psi^c_k(y_i)\psi^c_q(y_j)\rangle. \quad \text{(D9)}\end{aligned}$$

Using the parity transformation properties of the valence and conduction band extended states,[37] one can show that $\Psi^0_{S\bar{S}}(s)$ is of A_g symmetry

$$\Pi\ \Psi^0_{S\bar{S}}(s)\ \Pi^\dagger = \Psi^0_{S\bar{S}}(s). \quad \text{(D10)}$$

APPENDIX E: THE SSH/TLM JOINT DENSITY OF ELECTRONIC STATES

In the continuum model the optical energy spectrum is given by[35]

$$E_{cv}(k) = 2\Delta_0\sqrt{(k\xi_0)^2+1}. \quad \text{(E1)}$$

The joint density of electronic states per unit length becomes[63]

$$\rho_{cv}(x) \equiv \left|\frac{dE_{cv}(k)}{dk}\right|^{-1} = \rho^0_{cv}\frac{|x|}{\sqrt{|x^2-1|}} \equiv \rho^0_{cv}\frac{|x|}{Z}, \quad \text{(E2)}$$

with the joint density of electronic states prefactor given by[34]

$$\rho^0_{cv} = \frac{1}{2\Delta_0\xi_0} = \frac{1}{aW} = 6.6\times10^6\ \text{eV}^{-1}\,\text{cm}^{-1}. \quad \text{(E3)}$$

In Eq. (E2) we have defined

$$\begin{aligned}Z \equiv k\xi_0 &= \sqrt{|x^2-1|} \\ \Rightarrow dZ &= dx\ \frac{|x|}{Z} = \frac{1}{\rho^0_{cv}}\ dx\ \rho_{cv}(x). \quad \text{(E4)}\end{aligned}$$

From Eqs. (E2) and (E4) we see that a simple change of variables can be used to eliminate the singularity in the joint density of states

$$\int dx\ \rho_{cv}(x)\ G(x) = \rho^0_{cv}\int dZ\ G(Z) \quad \text{(E5)}$$

for an arbitrary function $G(x)$.

APPENDIX F: THE SSH/TLM ELECTRIC DIPOLE MOMENT MATRIX ELEMENT

In the TLM model the electric dipole moment matrix elements are defined in terms of the two-component spinor momentum operator $-i\hbar\sigma_3\partial/\partial x$ (Ref. 37)

$$\begin{aligned}f_{2,1} &= \langle\psi_2|\mathbf{y}|\psi_1\rangle \\ &= -i\left(\frac{\hbar}{m_e}\right)\frac{1}{\Delta_0}|M_x|\left[\frac{\Delta_0}{E^*_2-E_1}\right]\langle\psi_2|\sigma_3|\psi_1\rangle \quad \text{(F1)}\end{aligned}$$

where $|M_x| \sim \hbar/a$ is the momentum matrix element between two carbon p_z orbitals located on adjacent sites.[34]

1. Vertical interband transitions

$$\langle\psi^c_k|\sigma_3|\psi^v_k\rangle = \int_{-L/2}^{L/2} dy[U^{c*}_k U^v_k - V^{c*}_k V^v_k] = \frac{i}{|x|}. \quad \text{(F2)}$$

The vertical interband dipole moment matrix element has been determined previously;[34] it is expressed here in terms of the dimensionless complex optical energy parameter $x = E_{cv}(k)/2\Delta_0$

$$f_{cv}(x) = f^0_{cv}\frac{1}{|x|^2}, \quad \text{(F3)}$$

with the interband dipole moment matrix element prefactor given by

$$f^0_{cv} = \left(\frac{\hbar}{m_e}\right)\left[\frac{1}{\Delta_0}\right]|M_x| = 7.1\times10^{-8}\ \text{cm}. \quad \text{(F4)}$$

2. Nonvertical interband transitions

The nonvertical interband momentum matrix element is given by

$$\begin{aligned}\langle\psi^c_q|\sigma_3|\psi^v_k\rangle &= \int_{-L/2}^{L/2} dy\ e^{i(k-q)y}\ [U^{c*}_q U^v_k - V^{c*}_q V^v_k] \\ &\approx \text{sinc}\left(\frac{\Delta kL}{2}\right)\ \frac{i}{|x|}, \quad \text{(F5)}\end{aligned}$$

where

$$\Delta k \equiv q-k = \frac{m}{N}\ \frac{\pi}{2a}, \quad \text{(F6)}$$

where $\text{sinc}(u) \equiv \sin(u)/u$, m is the difference in the Bloch indices between states q and k, and $\pi/2a$ is the zone boundary. Using Eq. (F1), the interband electric dipole moment matrix element becomes

$$\begin{aligned}\langle\psi^c_q|\mathbf{y}|\psi^v_k\rangle &\approx f^0_{cv}\ \frac{1}{|x|^2}\ \text{sinc}\left(\frac{\Delta kL}{2}\right) \\ &= f^0_{cv}\ \frac{1}{|x|^2}\ \text{sinc}\left(m\frac{\pi}{4}\right). \quad \text{(F7)}\end{aligned}$$

Because of the alternating *gerade-ungerade* symmetry of the Bloch levels within the conduction and valence bands, a feature not contained within the TLM model, there is a relaxed interband selection rule for the infinite chain which simply states that m is even. The total transition strength is enhanced by the nonvertical terms

$$\begin{aligned}\sum_q\langle\psi^v_k|\mathbf{y}|\psi^c_q\rangle\langle\psi^c_q|\mathbf{y}|\psi^v_k\rangle &= f^2_{cv}(k)\left[1+2\sum_{n=0}^{\infty}\text{sinc}^2\left(m\frac{\pi}{4}\right)\right] \\ &+O(1/N^2) \approx 2\ f^2_{cv}(k)\ , \quad \text{(F8)}\end{aligned}$$

where $m = 4n+2$. Hence, for each independent complete set of states that we sum over, the relaxation of the vertical selection rule effectively doubles the interband transition strength.

3. Intraband or exciton-migration terms

The intraband electric dipole moment matrix elements are defined as

$$\langle\psi_q^{c,v}|\mathbf{y}|\psi_k^{c,v}\rangle = -i\ f_{cv}^0\left[\frac{\Delta_0}{E_q^{c,v*}-E_k^{c,v}}\right]\langle\psi_q^{c,v}|\sigma_3|\psi_k^{c,v}\rangle. \tag{F9}$$

Charge conjugation symmetry requires that

$$\langle\psi_q^c|\sigma_3|\psi_k^c\rangle = -\langle\psi_q^v|\sigma_3|\psi_k^v\rangle \tag{F10}$$

and

$$\mathrm{Re}[E_q^{c*}-E_k^c] = -\mathrm{Re}[E_q^{v*}-E_k^v]. \tag{F11}$$

The important terms occur near the band edge where the density of states is large. Here the energy can be expanded to yield its dependence on N

$$\begin{aligned}\epsilon_k &= \Delta_0\sqrt{(n/N)^2p^2+1}\\ &\approx \Delta_0\left[1+\frac{1}{2}\ (n/N)^2p^2\right],\end{aligned} \tag{F12}$$

where $p=\pi\xi_0/2a$ is the dimensionless TLM wave vector. Near the singularity at $2\Delta_0$, the real part of the energy denominator is given by

$$\begin{aligned}\Delta\epsilon_{q,k} \equiv \epsilon_q-\epsilon_k &= +(\epsilon_q^c-\epsilon_k^c) = -(\epsilon_q^v-\epsilon_k^v)\\ &= \Delta_0\ p^2\ \frac{m(m+2n)}{2N^2}.\end{aligned} \tag{F13}$$

The spinor momentum matrix element is given by

$$\langle\psi_q^c|\sigma_3|\psi_k^c\rangle = \mathrm{sinc}\left(\frac{\Delta kL}{2}\right)[U_q^{c*}U_k^c - V_q^{c*}V_k^c]. \tag{F14}$$

Near the band edge

$$\langle\psi_q^c|\sigma_3|\psi_k^c\rangle \approx \mathrm{sinc}\left(\frac{\Delta kL}{2}\right)\frac{1}{L}p\frac{m+2n}{2N}. \tag{F15}$$

a. The general case

$$\begin{aligned}E_q^{c*}-E_k^c &= \Delta\epsilon_{q,k}+\frac{i}{2}(\Gamma_q+\Gamma_k),\\ E_q^{v*}-E_k^v &= -\Delta\epsilon_{q,k}+\frac{i}{2}(\Gamma_q+\Gamma_k).\end{aligned} \tag{F16}$$

The intraband matrix elements can be written as follows:

$$\begin{aligned}\langle\psi_q^v|\mathbf{y}|\psi_k^v\rangle &= f_{\Delta k}\ e^{-i\phi_{\Delta k}},\\ \langle\psi_q^c|\mathbf{y}|\psi_k^c\rangle &= f_{\Delta k}\ e^{+i(\phi_{\Delta k}+\pi)},\end{aligned} \tag{F17}$$

where the magnitude and phase of the intraband electric dipole moment matrix element are given by

$$\begin{aligned}f_{\Delta k} &= f_{cv}^0 p\frac{m+2n}{2N}\ \mathrm{sinc}\left(m\frac{\pi}{4}\right)\\ &\quad\times\frac{2\Delta_0}{\sqrt{(\Delta\epsilon_{q,k})^2+\frac{1}{4}(\Gamma_q+\Gamma_k)^2}},\\ \phi_{\Delta k} &= \tan^{-1}\left[\frac{2\Delta\epsilon_{q,k}}{\Gamma_q+\Gamma_k}\right].\end{aligned} \tag{F18}$$

The factor of π which appears in the phase factor of the intra-conduction-band matrix element is a consequence of charge conjugation symmetry [see Eq. (F10)].

b. The case $\Gamma_k = \Gamma_q = 0$

If we neglect lifetime broadening effects, the intraband matrix element becomes

$$\begin{aligned}\langle\psi_q^c|\mathbf{y}|\psi_k^c\rangle &= \langle\psi_q^v|\mathbf{y}|\psi_k^v\rangle\\ &= -i\ \mathrm{sgn}(m)\ f_{cv}^0\ \mathrm{sinc}\left(m\frac{\pi}{4}\right)\frac{1}{p}\ \frac{N}{|m|}.\end{aligned} \tag{F19}$$

The sign difference between $\pm|m|$ terms leads to an exact cancellation of the exciton-migration terms.

c. The case $\Gamma_k \gg \Delta\epsilon_{q,k}$

If we assume that lifetime broadening effects dominate the energy denominator, i.e., $\Gamma_k \gg \Delta\epsilon_{q,k}$, the matrix elements become

$$\begin{aligned}\langle\psi_q^c|\mathbf{y}|\psi_k^c\rangle &= -f_{cv}^0\ p\ \frac{m+2n}{2N}\ \mathrm{sinc}\left(m\frac{\pi}{4}\right)\frac{\Delta_0}{\Gamma_k},\\ \langle\psi_q^v|\mathbf{y}|\psi_k^v\rangle &= +f_{cv}^0\ p\ \frac{m+2n}{2N}\ \mathrm{sinc}\left(m\frac{\pi}{4}\right)\frac{\Delta_0}{\Gamma_k},\end{aligned} \tag{F20}$$

where, as stated previously, the sign difference is a result of charge conjugation symmetry. It is clear from Eq. (F20) that finite lifetime effects reduce the amplitude of the exciton-migration terms, as the matrix elements go like $1/N$. By taking all combinations of third order intraband processes (vv, vc, cv, cc), it becomes apparent that the sign difference between the intra-conduction-band matrix element and the intra-valence-band matrix element leads, again, to an exact cancellation.

APPENDIX G: SSH/TLM MATRIX ELEMENT SUMMARY

1. Direct interband transition

$$\langle K_I|\mathbf{y}|G\rangle = \langle K_{II}|\mathbf{y}|K_I\rangle = \sqrt{2}\ f_{cv}(k) = \sqrt{2}\ f_{cv}^0\frac{1}{|x|^2}. \tag{G1}$$

2. Direct photoproduction of B_u symmetric $S\bar{S}$ configurations

$$\langle S\bar{S}^{\pm}|\mathbf{y}|G\rangle = \sqrt{2}\,\frac{1}{N}\,I_0^2\,f_{cv}^0\,\frac{1}{|w_0|} \times \sum_{k,q\neq k} e^{i(k+q)Y}\frac{1}{|x'|}\,G(s,k,q) \times|\Phi_0(s)|\,\delta_{k,-q}. \tag{G2}$$

3. Transitions involving free electron-hole pairs and A_g symmetric $S\bar{S}$ configurations

$$\langle S\bar{S}^0|\mathbf{y}|K_I'\rangle = \sqrt{2}\,\frac{1}{N}\,I_0^2\,f_{cv}^0\sum_{k,q\neq k} e^{i(k+q)Y}\frac{1}{(w_2^*-x')} \times\frac{1}{|x|}\,G(s,k,q)|\Phi_0(s)|\delta_{k,-q}\,\delta_{k,k'}. \tag{G3}$$

APPENDIX H: NUMERICAL CONSTANTS

$\Delta_0 = 0.9$ eV,
$|M_x| \sim \hbar/a = 5.5\times10^{-8}$ eV s/cm,
$\xi_0 = 7a = 8.4\times10^{-8}$ cm,
$f_{cv}^0 = (\hbar/m_e)\Delta_0^{-1}\,|M_x| = 7.1\times10^{-8}$ cm,
$W = 2\Delta_0\,(\xi_0/a) = 12.6$ eV,
$\sigma = L/V = 3.2\times10^{14}$ cm^{-2},
$\rho_{cv}^0 = (2\Delta_0\xi_0)^{-1} = 6.6\times10^{6}$ eV^{-1} cm^{-1},
$n = N/V = \sigma/a = 2.7\times10^{22}$ cm^{-3},
$\hbar/m_e = 1.16$ cm^2/s,
$\Gamma_k = \Gamma_s^{\pm} = \Gamma_s^0 = 0.10$ eV,
$e^2 = 1.44\times10^{-7}$ eVcm $= (300\text{ eV}/\text{V}_s)^2$,
$M_{S\bar{S}} = m_e[1 + 0.295\bar{K}_0^2]$.

[1] M. Sinclair, D. Moses, K. Akagi and A. J. Heeger, Phys. Rev. B **38**, 10 724 (1988).
[2] C. Halvorson, D. Moses, T. W. Hagler, Y. Cao, and A. J. Heeger, Synth. Met. **49-50**, 49 (1991).
[3] C. Halvorson, T. W. Hagler, D. Moses, Y. Cao, and A. J. Heeger, Chem. Phys. Lett. **200**, 364 (1992).
[4] T. Kaino, K. Kubodera, H. Kobayashi, T. Kurihara, S. Saito, T. Tsutsui, S. Tokito, and H. Murata, Appl. Phys. Lett. **53**, 2002 (1988).
[5] T. Kanetake, K. Ishikawa, T. Hasegawa, T. Koda, K. Takeda, M. Hasegawa, K. Kubodera, and H. Kobayashi, Appl. Phys. Lett. **54**, 2287 (1989).
[6] F. Kajzar, G. Ruani, C. Taliani, and R. Zamboni, Synth. Met. **37**, 223 (1990).
[7] J. A. Osaheni, S. A. Jenekhe, H. Vanherzeele, J. S. Meth, Yan Sun, and A. G. MacDiarmid, J. Phys. Chem. **96**, 2830 (1992).
[8] A. K. Agrawal, S. A. Jenekhe, H. Vanherzeele, and J. S. Meth, J. Phys. Chem. **96**, 2837 (1992).
[9] G. P. Agrawal, C. Cojan, and C. Flytzanis, Phys. Rev. B **17**, 776 (1978).
[10] Chang-qin Wu and Xin Sun, Phys. Rev. B **42**, 9736 (1990).
[11] X. Sun, K. Nasu, and C. Q. Wu, Phys. Rev. B **54**, 170 (1992).
[12] Weikang Wu, Phys. Rev. Lett. **61**, 1119 (1988).
[13] Weikang Wu and S. Kivelson, Synth. Met. **28**, D575 (1989).
[14] J. Yu, B. Friedman, P. R. Baldwin, and W. P. Su, Phys. Rev. B **39**, 12 814 (1989).
[15] T. W. Hagler and A. J. Heeger, Chem. Phys. Lett. **189**, 333 (1992).
[16] L. Lauchlan, S. Etemad, T. C. Chung, A. J. Heeger, and A. G. MacDiarmid, Phys. Rev. B **24**, 3701 (1981).
[17] S. Etemad, T. Mitani, M. Ozaki, T. C. Chung, A. J. Heeger, and A. G. MacDiarmid, Solid State Commun. **40**, 75 (1981)
[18] D. Moses, A. Feldblum, E. Ehrenfreund, A. J. Heeger, T. C. Chung, and A. G. MacDiarmid, Phys. Rev. B **26**, 3361 (1982).
[19] T. W. Hagler, Ph.D. dissertation, University of California, Santa Barbara, 1991.
[20] G. Leising, Phys. Rev. B **38**, 10 313 (1988).
[21] J. Orenstein, G. L. Baker, and Z. Vardeny, Phys. (Paris) Colloq. **44**, C3-407 (1983).
[22] S. D. Phillips, R. Worland, G. Yu, T. W. Hagler, R. Freedman, Y. Cao, V. Yoon, J. Chiang, W. C. Walker, and A. J. Heeger, Phys. Rev. B **40**, 9751 (1989).
[23] T. W. Hagler, K. Pakbaz, K. F. Voss, and A. J. Heeger, Phys. Rev. B **44**, 8652 (1991).
[24] B. R. Weinberger, C. B. Roxlo, S. Etemad, G. L. Baker, and J. Orenstein, Phys. Rev. Lett. **53**, 86 (1984).
[25] Y. Cao, P. Smith, and A. J. Heeger, Polymer **32**, 1210 (1991).
[26] S. D. Phillips, Ph.D. dissertation, University of California, Santa Barbara, 1989.
[27] W. P. Su and J. R. Schrieffer, Proc. Natl. Acad. Sci. U.S.A. **77**, 5626 (1980)
[28] J. P. Sethna and S. Kivelson, Phys. Rev. B **26**, 3513 (1982).
[29] J. P. Sethna and S. Kivelson, Phys. Rev. B **27**, 7798 (1983).
[30] Zhao-bin Su and Lu-Yu, Phys. Rev. B **27**, 5199 (1983).
[31] A. Auerbach and S. Kivelson, Phys. Rev. B **33**, 8171 (1986).
[32] J. Yu, H. Matsuka, and W. P. Su, Phys. Rev. B **37**, 10 367 (1988).
[33] B. Henderson and G. F. Imbusch, *Optical Spectroscopy of Inorganic Solids* (Clarendon Press, Oxford, 1989).
[34] W. P. Su, J. R. Schrieffer, and A. J. Heeger, Phys. Rev. Lett. **42**, 1698 (1979).
[35] H. Takayama, Y. R. Lin-Liu, and K. Maki, Phys. Rev. B **21**, 2388 (1980).
[36] S. A. Brazovskiĭ and N. N. Kirova, Pis'ma Zh. Eksp. Teor. Fiz. **33**, 6 (1981) [JETP Lett. **33**, 4 (1981)].
[37] K. Fesser, A. R. Bishop, and D. K. Campbell, Phys. Rev. B **27**, 4804 (1983).
[38] G. H. Wannier, Phys. Rev. **52**, 191 (1937).
[39] G. Dresselhaus, Phys. Chem. Solids **1**, 14 (1956).
[40] R. J. Elliott, Phys. Rev. **108**, 1384 (1957).
[41] C. Sirtori, F. Capasso, D. L. Sivco, and A. Y. Cho, Phys. Rev. Lett. **68**, 1010 (1992)
[42] A. J. Heeger, S. Kivelson, J. R. Schrieffer, and W. P. Su, Rev. Mod. Phys. **60**, 781 (1988)
[43] B. J. Orr and J. F. Ward, Mol. Phys. **20**, 513 (1971).
[44] D. Yaron and R. Silbey, Phys. Rev. B **45**, 11 655 (1992).
[45] D. E. Aspnes and J. E. Rowe, Phys. Rev. B **5**, 4022 (1972).
[46] Z. G. Soos, G. W. Hayden, and P. C. M. Williams, in *Conjugated Polymeric Materials: Opportunities in Electronics, Optoelectronics and Molecular Electronics*, Vol. 182

of *NATO Advanced Study Institute, Series E: Applied Sciences*, edited by J. L. Bredas and R. R. Chance (Kluwer, Dordrecht, 1990).

[47]R. Ball, W. P. Su, and J. R. Schrieffer, Phys. (Paris) Colloq. **44**, C3-429 (1983).

[48]N. Suzuki, M. Ozaki, S. Etemad, A. J. Heeger, and A. G. MacDiarmid, Phys. Rev. Lett. **45**, 1209 (1980).

[49]S. Kivelson, T. K. Lee, Y. R. Lin-liu, I. Peschel, and Lu Yu, Phys. Rev. B **25**, 4173 (1982).

[50]A. Feldblum, J. H. Kaufman, S. Etemad, A. J. Heeger, T. C. Chung, and A. G. MacDiarmid, Phys. Rev. B **26**, 815 (1982).

[51]In order to force the lattice with nonlinear zero-point motion to conserve oscillator strength, we have included the empirical separation dependent mass correction factor $M_{S\bar{S}} \approx m_e(1+0.295\bar{K}_0^2)$. For a well-separated $S\bar{S}$ pair, this factor represents a 30% correction to the rigid-lattice value, and in the limit of infinite confinement, $M_{S\bar{S}} \Rightarrow m_e$, as it must. When integrated over the ground state lattice wave function, $M_{S\bar{S}}$ *reduces* the magnitude of the $S\bar{S}$ contribution to the linear and nonlinear susceptibility by 10%.

[52]M. Tinkham, *Group Theory and Quantum Mechanics* (McGraw-Hill, New York, 1964).

[53]Weikang Wu and S. Kivelson, Phys. Rev. B **33**, 8546 (1986).

[54]S. Kivelson and Weikang Wu, Phys. Rev. B **34**, 5423 (1986).

[55]M. F. Granville, B. E. Kohler, and J. B. Snow, J. Chem. Phys. **75**, 3765 (1981).

[56]W. P. Su, Solid State Commun. **42**, 497 (1982).

[57]J. E. Hirsch and E. Fradkin, Phys. Rev. Lett. **49**, 402 (1982).

[58]R. H. Mc Kenzie and J. W. Wilkins, Phys. Rev. Lett. **69**, 1085 (1992).

[59]A. Takahashi, Phys. Rev. B **46**, 11 550 (1992).

[60]The Gaussian form is approximate for the ground-state potential and $V(s)$ deviates from quadratic at large s, approaching $4\Delta_0/\pi$ (Ref. 32). As a consequence, use of the Gaussian underestimates the magnitude of $|\phi_0(s)|^2$ for large s.

[61]J. Chen, T. C. Chung, F. Moraes, and A. J. Heeger, Solid State Commun. **53**, 757 (1985).

[62]F. Moraes, J. Chen, T. C. Chung, and A. J. Heeger, Synth. Met. **11**, 271 (1985).

[63]F. Wooten, *Optical Properties of Solids* (Academic Press, New York, 1972).

[64]The electric field induced change to the extinction coefficient is given by $\Delta\kappa = (2\pi/|N_0|^2)[n_0\chi^{(3)}_{\rm Im}(\omega) - \kappa_0\chi^{(3)}_{\rm Re}(\omega)]\mathbf{F}^2$, where n_0 and κ_0 are the linear optical coefficients in the absence of the applied field $\mathbf{F}$. Below the first optical resonance n_0 dominates and therefore an induced absorption (positive $\Delta\kappa$) requires that the imaginary component of the nonlinear susceptibility is positive.

[65]C. V. Shank, R. Yen, J. Orenstein, and G. L. Baker, Phys. Rev. B **28**, 6095 (1983).

[66]B. S. Hudson, B. E. Kohler, and K. Schulten, in *Excited States*, edited by K. C. Lim (Academic Press, New York, 1982), Vol. 6, p. 1.

[67]P. C. M. Mc Williams, G. W. Hayden, and Z. G. Soos, Phys. Rev. B **43**, 9777 (1991).

[68]N. F. Colaneri, D. D. C. Bradley, R. H. Friend, P. L. Burn, A. B. Holmes, and C. W. Spangler, Phys. Rev. B **42**, 11 670 (1990).